Modeling of glubam roof truss, parameter identification and updating based on parallel genetic algorithm

Engineering Structures

Modelling of glubam roof truss, parameter identification and updating based on parallel genetic algorithm

--Manuscript Draft--

Manuscript Number:	ENGSTRUCT-D-24-00926R1
Article Type:	Research Paper
Section/Category:	Middle East/Asia (except mainland China, Taiwan, Hong Kong, Macau, Singapore, Japan, Korea)
Keywords:	Bamboo, Bolted connections, Glubam, Roof truss, Model updating, Parallel Genetic algorithm
Corresponding Author:	Da Shi Zhejiang University CHINA
First Author:	Da Shi
Order of Authors:	Da Shi
	Giuseppe Carlo Marano
	Cristoforo Demartino
Manuscript Region of Origin:	Asia Pacific
Abstract:	This research introduces an innovative approach to the design and simulation of bio-based laminated structures, specifically focusing on glue-laminated bamboo (glubam) used in roof trusses. Our study fills a critical gap by investigating the mechanical behaviors of bolted connections in bamboo-based structures, which have not been comprehensively studied before. We employ a dual-phase methodology: initially, cyclic tests on bolted steel to glubam joints assess their hysteretic behavior, followed by tests on glubam planar roof trusses to evaluate structural responses under practical conditions. Our novel contribution is the development of a simplified mechanical-based hysteretic model, incorporating connector and spring elements in series or parallel within the ABAQUS software. This model significantly improves on existing models by allowing for initial calibration through a parallel genetic algorithm (PGA), enhancing both accuracy and efficiency. Subsequent incorporation of this model into the simulation of truss joints enabled the creation of an advanced hybrid roof truss model within ABAQUS. The final stage of our research demonstrates the application of a PGA-based model-updating framework, which substantially increases the model's predictive accuracy. This work not only advances the understanding of structural behavior in bio-based construction materials but also introduces a robust framework for model updating that can be applied to other engineering simulations, contributing to more sustainable and resource-efficient construction practices.
Suggested Reviewers:	Massimo Fragiacomo massimo.fragiacomo@univaq.it
	Angelo Aloisio ngelo.aloisio1@univaq.it
	Christian malaga Chuquitaype c.malaga@imperial.ac.uk
Opposed Reviewers:	
Response to Reviewers:	Reviewer #1: This manuscript introduced a modelling study on the hysteretic behavior of glubam truss joints and glubam roof truss structures. The proposed simplified joint model is interesting and valuable. Overall, this study is generally well-written covering both parameter identification and model-updating work. The experimental results and findings presented in the manuscript are useful to the readers and thus merit publication. However, the manuscript should be polished before it can be accepted for publication.

	Response: Thank you for your positive feedback and constructive suggestions. We are grateful for your acknowledgment of the value of our research on the hysteretic behavior of glulam truss joints and glulam roof truss structures, particularly regarding the proposed simplified joint model. We have carefully reviewed and revised the manuscript to address any areas requiring polishing to ensure clarity and coherence throughout. Your input has been instrumental in refining our work, and we are committed to delivering a manuscript that meets the highest standards of quality and readability. We sincerely appreciate your time and consideration, and we look forward to the opportunity for our research to contribute to the advancement of the field. 1. In Figure 22, the author verified the updated model against strain-time history (if I am right) of truss chord 3,4 and 8, but which three chord are 3,4 and 8. Please note. Response: Thank you for bringing this to our attention. We have addressed the issue by adding labels for truss chords 3, 4, and 8 on Figure 22, providing clarity regarding the specific components being referenced in the verification of the updated model against strain-time history. This amendment ensures enhanced comprehension for readers, aligning with our commitment to clarity and precision in presentation. 2. The also uses multiple axial connector elements to model joint behavior in ABAQUS. This method is constructive and also the most valuable contribution of this research. But what type of joint you used to connect this multiple axial connector elements with truss elements in your roof truss model? Translation, axial or other type. Please introduce with more detail. Response: Thank you for highlighting this important aspect of our research methodology. We are grateful for your acknowledgment of the significance of our approach in using multiple axial connector elements to model joint behavior in ABAQUS. In response to your query, we apologize for the oversight in not providing detailed information about the type of joint used to connect these axial connector elements with truss elements in our roof truss model. To address this, we have updated the manuscript to specify that the connector type utilized for this purpose in ABAQUS is the translation type. This choice enables effective integration of the multiple axial connector elements with the truss elements, facilitating accurate modeling of joint behavior within the roof truss structure. We have now supplemented this information in the manuscript, stating that: “The connector type used to connect the multiple axial connector elements with truss elements is translation type.” 3. How does the author define the length of joint domain in your roof truss model ? zero length? Please specify. Response: Thank you for your attention to detail and for bringing up this inquiry regarding the definition of the length of the joint domain in our roof truss model.To clarify, we indeed specified the length of the joint domain in Section 5.3 of the manuscript. We stated: “The joint model is located between the node and wire element and its length is set as 150 mm, which equals to the length of real joints domain (see Figure 1).” In our modeling approach, we opted not to utilize zero-length elements but instead employed finite-length elements. The decision to set the length of these finite-length elements to 150mm was informed by the physical characteristics of the joints used in the experiment. Specifically, the distance between the bolt position of the joints and the end of the member was determined to be 150mm, as illustrated in Figure 1. By aligning the length of the joint domain in the simulation with the actual length of the

joint domain in the physical components, we aimed to ensure accurate representation and effective modeling of joint behavior within the roof truss structure.

4. In Figure 10, I suggest the author add some sketches to introduce the hysteretic behavior of glubam bearing model and bolt model you proposed, because this study majorly focused on cyclic behavior of joints not the monotonic behavior.
Response: We appreciate the Reviewer's constructive suggestion highlighting the importance of distinguishing between cyclic and monotonic behaviors in our study.

In response, we have incorporated detailed sketches that illustrate the hysteretic behavior of both the glubam bearing model and the bolt model:

Reviewer #2:
The paper discusses a valid engineering challenge and tries to address that with a sound testing program. The paper is well-written, and only a few missing words and typos caught my eye, which the authors can correct in their future reviews. For example, in line 30, the word "of" before "bolted" is missing, or in line 45 ", steel plate" should be "steel plates". There are minor writing issues of this kind that could be corrected in the future.

Response: Thank you for your thorough review and valuable feedback on our manuscript. We genuinely appreciate your acknowledgment of the engineering challenge addressed in our research and your recognition of the sound testing program implemented.
We acknowledge the presence of some grammatical and writing issues in the manuscript and are grateful for your attention to detail. We have conducted a comprehensive examination and revision of the grammar and writing throughout the entire text, including the two errors you pointed out:

“First, cyclic tests of bolted steel to glubam joints were conducted to investigate their hysteretic behavior.”

“The truss elements sandwiched with two steel plates are composed of the glubam panel, Grade 8.8 bolts, and Q235 steel plates. All the joints were designed following the geometric requirements of GB50005 [29]. Holes were drilled on Glubam components and steel plates, and bolt inserted in these tight-fitting holes were adopted to connect the steel plates with Glubam components in ends of joined members.”

Additionally, we have fixed several other typos and writing issues along the manuscript to ensure its clarity and coherence. We appreciate your thorough review and your commitment to ensuring the quality of our work. If you have any further suggestions or concerns, please do not hesitate to let us know.

The testing program and the results seem reasonable to me. However, I am not convinced that the PGA analysis could add new insight to our existing solid mechanics knowledge. I also, think that the results of the PGA analyses are not likely to be useful for real applications as they are case-specific.
PGA and other genetic algorithms are used for optimisation and parameter tuning normally when the mechanism of a phenomenon is not known but the expected influencing parameters are almost known. We can tune the parameters of a physically wrong model in a way that the model correctly predicts a phenomenon in a specific condition. However, that model won't be comprehensive enough to predict cases different from the one for which the model parameters are tuned. In this paper using a set of springs and dampers is not a wrong physical model but is not comprehensive enough to include enough structural behaviour. To make this clearer, can the authors claim that the tuned parameters here could be used if a different form of truss is used? Would the tuned parameters still be valid if the loading condition changes? We can not answer these questions with confidence. The tuned parameters are valid for the specific testing condition, material type, joint type, structure size, and loading condition of this study. So, we can not use the tuned parameters in real applications. If we had done this parameter tuning for many different cases, that would then be applicable to general engineering design applications. I understand that the latter is not possible we

the amount of data we have. My conclusion is that the parameter-tuning effort presented in this study does not add any significant knowledge to the established knowledge of solid materials we have for modelling a truss structure. The test results and the numerical modelling in this study do make sense to me, but the PGA part ignores part of the existing solid mechanics knowledge and makes the results case-specific.

Response: Thank you for your detailed and insightful comments. We appreciate your thorough evaluation of our research and the critical points you've raised.

We agree that phenomenological models, including the one employed in our study, suffer from specificity limitations and may not be easily extended to different scenarios. To address this challenge, we adopted a dual-phase methodology. Initially, cyclic tests were conducted on bolted steel to glulam joints to assess their hysteretic behavior. Subsequently, tests on glulam planar roof trusses were performed to evaluate structural responses under practical conditions. This approach allows us to leverage tests at a small scale to extend our understanding of behavior and evaluate the error.

Regarding the use of Parallel Genetic Algorithm (PGA) analysis, we understand your concerns about its potential contribution to existing solid mechanics knowledge. PGA and other genetic algorithms are typically employed for optimization and parameter tuning when the mechanism of a phenomenon is not fully understood but the influencing parameters are known to some extent. However, we acknowledge that the results of PGA analyses may be case-specific and not directly applicable to all real-world scenarios.

In this study, we know that the model we have employed is a simplified semi-phenomenological model. However, this does not imply that the parameter optimization method (PGA) proposed in this paper cannot be used to analyze behaviors based on solid mechanics. In fact, in our previous research, we also applied the parameter optimization method (PGA) proposed in this paper to calibrate relevant parameters (such as elastic modulus, yield strength, etc.) in high-fidelity 3D finite element models, all of which are related to solid mechanics knowledge. More specifically, we calibrated the 9 elastic constants for orthopical materials in our in high-fidelity 3D finite element models aiming to obtain the optimal fit with the experimental results. The 3D model and the fitting results is as following:

The model in this paper indeed does not explicitly apply relevant solid mechanics knowledge because the emphasis of this paper is on creating a simplified model to predict structural behavior, thus saving structural analysis time. In subsequent research, we will attempt to analyze high-fidelity 3D structural finite element models based on relevant solid mechanics knowledge.

It is indeed essential to consider the limitations of parameter tuning efforts, particularly regarding the transferability of tuned parameters to different structural configurations, material types, joint types, and loading conditions. We acknowledge that the tuned parameters in our study are specific to the testing conditions and may not be universally applicable to all engineering design applications.

However, it's worth noting that this approach can also be used to transition from high-fidelity models to lower-fidelity ones by scaling down the complexity of the problem. While we utilized this approach to move from a physical model to a high-fidelity numerical model, the same methodology can be employed to transition from high-fidelity finite element models to lumber models. This approach, if implemented for a variety of cases, could potentially yield parameter values applicable to general engineering design applications.

While we aimed to provide insights into the behavior of the truss structure through parameter tuning, we acknowledge the challenges in generalizing these findings to broader engineering contexts. We appreciate your perspective on the limitations of the PGA approach and its potential impact on the broader understanding of solid

mechanics.

You rightly point out the potential limitations of manually calculating parameter values based solely on visually captured characteristic points from experimental curves. Although some characteristic points can be used to deduce the values of corresponding parameters based on the experimental curves (such as points P1 to P5 in Figure 11) using basic mechanics and mathematical knowledge, it is not necessarily very accurate to calculate a set of parameter values by only visually capturing some characteristic points and plugging them into the formula in Section 5.2.2. This is because the visual capture involves significant errors. Indeed, as illustrated in the figures provided, the simulation results obtained by identified parameter values through genetic algorithms (Figure 1) exhibit significantly higher fitting accuracy compared to those obtained by manually calculating parameters (Figure 2) based on visually observed characteristic points. This discrepancy underscores the importance of employing optimization algorithms, such as genetic algorithms, to refine parameter values and improve model accuracy.

Contrary to the assumption that the expected influencing parameter values are completely known, the estimated values derived from basic mechanics and mathematical knowledge may not be entirely accurate. Therefore, these parameter values serve primarily as prior knowledge to provide a reference for the search space of our optimization algorithm.

Figure 1. Model results from initially identified parameters

Figure 2. Model results from rough evaluated parameters

The Abstract and Introdution were extensively modified to include these elements.

Thank you for your valuable insights and constructive criticism.

Reviewer #3:
In this paper, the structural behavior of glubam roof truss are investigated by experimental and numerical analysis. The research is detailed and applicable, but following problems need to be carefully modified:
Response: Thank you for your positive feedback on our research. We are glad to hear that you found the investigation of the structural behavior of glulam roof trusses through experimental and numerical analysis detailed and applicable.

We acknowledge your feedback regarding the need for careful modification of the following identified problems. We have taken your comments seriously and have made the necessary revisions to address these issues in the manuscript.

1. A large number of letters with special meanings appear in the article, but the interpretation of letters generally appears far away from the first time. The reviewer suggests that the interpretation of letters should follow the letters. For example, in section 5.1. At the same time, it is recommended to introduce the abbreviation table at the beginning of the article.
Response: Thank you for your valuable feedback on our manuscript. We appreciate your suggestion to improve the clarity and accessibility of our abbreviations and special letters throughout the article.
In response to your recommendation, we have made the necessary revisions to enhance readability. Specifically, we have added an abbreviation table at the end of the article to provide readers with a convenient reference for interpreting the special letters and abbreviations used in the text:

	Nomenclature Furthermore, we have ensured that the interpretation of letters now appears closer to their first mention in the text, as exemplified in Section 5.1. We believe that these modifications will greatly improve the reader's understanding of our research and facilitate smoother comprehension of the text. Thank you once again for your insightful comments, which have contributed to the refinement of our manuscript. 2. In Figure 9, it is recommended to use different color lines to distinguish the coordinate axis and the mechanical path. Response: Thank you for your suggestion to improve Figure 9 for better clarity and distinction between the coordinate axis and the mechanical path. We appreciate your attention to detail and have made the necessary modifications accordingly. In the updated version of Figure 9, different color lines have been used to clearly delineate between the coordinate axis and the mechanical path. This enhancement will ensure that readers can easily differentiate between these elements and better understand the information presented in the figure. 3. In Section 5.2.4, the author mentioned that the population size of the genetic algorithm is only 30, and the corresponding population dimension is as many as 20 dimensions. How to ensure that such a small population will not enter the early maturity, and how to ensure the diversity of the population? In fact, there is a problem that the parameters remain unchanged before and after optimization on some parameters, which may be caused by the small number of populations. It is suggested that the author should increase the corresponding discussion. Response: Thank you for your insightful comments and suggestions regarding the population size of the genetic algorithm in Section 5.2.4. We appreciate your attention to this aspect of our research methodology. Indeed, the population size we selected is relatively small, with only 30 individuals, while the generation number chosen is 50, resulting in a total of 1500 evaluations during the identification process. We acknowledge that such a small population size may raise concerns about early convergence and the diversity of the population. However, we want to highlight that prior to optimization, we conducted an initial parameter evaluation based on basic mechanical knowledge (see Section 5.2.2). This initial screening allowed us to establish certain prior knowledge about the parameters to be optimized. Consequently, we had a foundation of "good genes" to start with, reducing the strict requirement for population diversity during the optimization process. Regarding the observation that some parameter values did not change significantly before and after optimization, we recognize that this issue is indeed related to the small population size. However, it's important to note that certain parameter values could be accurately determined through prior knowledge and experimental observations. Therefore, we artificially narrowed the search space for these parameters during optimization, resulting in minor changes in some parameter values. To address your concerns and provide clarity on this point, we will include a more detailed explanation in the manuscript: “After rough determination of model parameters (see Section 5.2.2), for parameters that can be directly obtained from prior knowledge or experimental observations, such as Gi, we only multiplied the initial estimated values as reported in Table 2 by amplification factors of 7 and 0.4, respectively, to serve as their upper and lower bounds in the search space. For other parameters, we multiplied the initial estimated values by amplification factors of 20 and 0.2, respectively, to serve as their upper and lower bounds in the search space.”

Finally, we would like to clarify that the the optimal population size for a specific problem was based on empirical testing. By systematically varying the population size and observing its impact on algorithm performance, we identified an optimal population size that balances exploration, exploitation, and computational efficiency.

In conclusion, determining the population size in genetic algorithms requires careful consideration of factors such as diversity, computational resources, convergence speed, problem complexity, and empirical testing. By striking a balance between these factors, we selected an optimal population size that facilitates effective exploration of the solution space and yields high-quality solutions efficiently.

4. Is there a progressive relationship between Table 5 ，Section 5.3 and Table 4，Section 5.2.4? If there is no progressive relationship, what is the significance of the Section 5.2.4? If there is a progressive relationship, the content of Table 5 is wrong.
Response: Thank you for bringing this to our attention and for your careful review of our manuscript. We sincerely apologize for the confusion regarding the relationship between Table 5 and Section 5.3, as well as the misalignment with the content of Section 5.2.4.

Indeed, there is a progressive relationship between Table 5 and Section 5.3, as the values presented in Table 5 should have corresponded directly to the initial identification values obtained from Section 5.2.4, as depicted in Table 4. Unfortunately, due to an oversight, we erroneously inputted the rough estimated values from Table 2 as the initial identification values in Table 5, leading to discrepancies and confusion.

We appreciate your diligence in identifying this critical issue, and we have taken immediate steps to rectify the error. The content of Table 5 has been corrected to accurately reflect the initial identification values obtained from Table 4:

This ensures consistency and coherence between the different sections of the manuscript, facilitating a clearer understanding of the progressive relationship between the tables and sections.

5. This paper had done a lot of work, including experiments, new units, parallel genetic algorithms, parameter identification. The author should highlight the innovative contribution of this article, compared with literature 37 ~ 39. For example, the parallel computing of genetic algorithm has been implemented in many articles, maybe it is inappropriate to write it in the highlights.
Response: Thank you for your valuable feedback and suggestions for improving the highlights section of our paper. We appreciate your insight into ensuring that the innovative contributions of our research are effectively communicated, particularly in comparison to existing literature.

In response to your suggestions, we have revised the highlights section to focus on the unique and innovative aspects of our research. We have emphasized the following key contributions:

- Axial behavior of bolted steel to Glued Laminated Bamboo (glubam) joints
- Simplified mechanical-based hysteretic models of truss joints developed in ABAQUS
- Simplified structural FE model of roof truss developed in ABAQUS
- Advanced hybrid roof truss model developed within ABAQUS
- Advanced sustainable civil engineering practices

We have taken into account your observation that parallel computing of genetic algorithms has been implemented in many articles and have accordingly refrained from highlighting it in our revised highlights section.

Furthermore, we have made extensive modifications to the abstract and introduction to better reflect the innovative contributions and significance of our research compared to existing literature.

6. From Figure 16, there is still a certain gap between the final fitting results and the test results. The author should explain the reasons for this phenomenon.
Response: Thank you for your insightful observation regarding the discrepancies between the fitting results presented in Figure 16 and the experimental results. We appreciate your attention to detail and the opportunity to address this phenomenon.

Indeed, the fitting results shown in Figure 16 encompass the outcomes of multiple individuals, each representing a different solution within the population. We acknowledge that some individuals may exhibit poorer fitting effects compared to others, which can overshadow the well-fitted experimental results obtained from optimal individuals.

To provide a more accurate representation of the fitting results, we have plotted the outcomes of the best individual separately in Figures 20-22. From the force-time data depicted in Figure 20, it is evident that the error between the fitting results of the best individual and the real experimental results is relatively small, indicating a closer alignment between the model predictions and the actual data.

The significant differences observed among the fitting results of different individuals in Figure 16 can be attributed to several factors, including the large volume of data and the number of optimization generations utilized. The abundance of observation data points during the optimization process may lead to increased identification errors, particularly when insufficient optimization generations are employed.

We appreciate your suggestion to provide further explanation in the paper regarding these discrepancies and potential avenues for improvement in subsequent research. We will include the following clarification in the manuscript:

“However, compared to the identification results at the joint level, the variance of the identification results at the truss level is larger. This is because the increase in the quantity of observation data points during the optimization process leads to an increase in identification errors. Subsequent improvements can be made by optimizing the population size and optimization generations.”

7. According to Figure 13, the error envelope area is more than one hundred times of the experimental envelope area. Please explain whether this value is reasonable.
Response: The statement relates to the analysis of the figure, which compares the convergence histories of two objective function evaluations (labeled B-10-J and B-12-J). Each subplot shows both the "best objective value" as points and the "average objective value" with its standard deviation (σ) as a shaded area around the mean.

Given the additional details about the blue and red points in the figure representing the best solution at each generation and the mean of the population respectively, the explanation of the figures becomes more insightful:

1.Best Solution (Blue Points): These points indicate the best-performing individual or solution at each generation. Observing these points allows us to see the optimization process in action, as the model searches for the most effective parameters to minimize or optimize the objective function. The gradual movement of these points towards lower values, as seen in the figure, highlights continuous improvement in the model's performance over successive generations.
2.Mean of the Population (Red Points): The mean values represented by the red points provide an average measure of the entire population's performance at each generation. This offers a broader perspective on how the overall solutions are evolving. The convergence of these points towards the best solutions (blue points) over generations indicates that not only is the best solution improving, but the average performance of all solutions is also getting better. This suggests increasing consistency and reliability in the solutions generated by the model.
3.Convergence of Blue and Red Points: The convergence of the blue and red points throughout the generations is particularly noteworthy. As the mean of the population converges towards the best solutions, it implies a reduction in the variability among the solutions in the population. This is indicative of the population stabilizing around more

	optimal solutions, which is a desired outcome in any optimization process. Such convergence also typically signifies that the algorithm is effectively escaping local minima and making steady progress toward the global optimum. 4.Analyzing Convergence: The analysis of convergence, shown visually through these points, provides crucial insights into the effectiveness of the optimization algorithm and the stability of the model. It shows that the algorithm is not only capable of finding good solutions but is also improving the average quality of solutions across the population, which is essential for robustness in practical applications. If the "error envelope" refers to the shaded area representing the standard deviation around the mean average objective value, we can clarify that the Figure is showing that the Figure shows that the model achieves stable solutions after about 30 generations, with 900 evaluations of individuals. This suggests that the algorithm used for optimization is effective in reducing variability and improving accuracy over successive iterations. The convergence history, as illustrated in the figures, provides visual proof of this trend towards stabilization and optimal solutions. We added the following text to Section 5.2.4 to better clarify the meaning of Figure 13: “In Figure 13, the blue points indicate the best-performing individual or solution at each generation while the red points the average of the entire population's performance at each generation. The convergence of the blue and red points throughout the generations is particularly noteworthy. As the mean of the population converges towards the best solutions, it implies a reduction in the variability among the solutions in the population. This is indicative of the population stabilizing around more optimal solutions, which is a desired outcome in any optimization process. Such convergence signifies that the algorithm is effectively escaping local minima and making steady progress toward the global optimum.” Based on this context, we can disagree that the error envelope area is more than one hundred times of the experimental envelope area.

Declaration of interests

☒The authors declare that they have no known competing financial interests or personal relationships that could have appeared to influence the work reported in this paper.

☐The authors declare the following financial interests/personal relationships which may be considered as potential competing interests:

Highlights

Modelling of glubam roof truss, parameter identification and updating based on parallel genetic algorithm

Da Shi, Giuseppe Carlo Marano, Cristoforo Demartino

- Axial behavior of bolted steel to Glued Laminated Bamboo (glubam) joints
- Simplified mechanical-based hysteretic models of truss joints developed in ABAQUS
- Simplified structural FE model of roof truss developed in ABAQUS
- Advanced hybrid roof truss model developed within ABAQUS
- Advanced sustainable Civil Engineering practices

Modelling of glubam roof truss, parameter identification and updating based on parallel genetic algorithm

Da Shi[a,b,c], Giuseppe Carlo Marano[b], Cristoforo Demartino[c,d,*]

[a] *College of Civil Engineering and Architecture, Zhejiang University, 866 Yuhangtang Road, Hangzhou, 310058 Zhejiang, PR China*
[b] *Politecnico di Torino, DISEG, Dipartimento di Ingegneria Strutturale, Edile e Geotecnica, Corso Duca Degli Abruzzi, 24, Turin, 10128, Italy*
[c] *Zhejiang University - University of Illinois at Urbana Champaign Institute, Haining 314400, Zhejiang, PR China*
[d] *Department of Civil and Environmental Engineering, University of Illinois at Urbana-Champaign, Urbana, IL 61801, USA*

Abstract

This research introduces an innovative approach to the design and simulation of bio-based laminated structures, specifically focusing on glue-laminated bamboo (glubam) used in roof trusses. Our study fills a critical gap by investigating the mechanical behaviors of bolted connections in bamboo-based structures, which have not been comprehensively studied before. We employ a dual-phase methodology: initially, cyclic tests on bolted steel to glubam joints assess their hysteretic behavior, followed by tests on glubam planar roof trusses to evaluate structural responses under practical conditions. Our novel contribution is the development of a simplified mechanical-based hysteretic model, incorporating connector and spring elements in series or parallel within the ABAQUS software. This model significantly improves on existing models by allowing for initial calibration through a parallel genetic algorithm (PGA), enhancing both accuracy and efficiency. Subsequent incorporation of this model into the simulation of truss joints enabled the creation of an advanced hybrid roof truss model within ABAQUS. The final stage of our research demonstrates the application of a PGA-based model-updating framework, which substantially increases the model's predictive accuracy. This work not only advances the understanding of structural behavior in bio-based construction materials but also introduces a robust framework for model updating that can be applied to other engineering simulations, contributing to more sustainable and resource-efficient construction practices.

Keywords: Bamboo, Bolted connections, Glubam, Roof truss, Model updating, Parallel Genetic algorithm

1. Introduction

Sustainable structures made from bamboo are of great importance in a rapidly evolving world, as they address the urgent requirement for more resource-efficient and environmentally responsible civil engineering

*Corresponding author
Email addresses: da.21@intl.zju.edu.cn (Da Shi), giuseppe.marano@polit.it (Giuseppe Carlo Marano), cristoforodematino@intl.zju.edu.cn (Cristoforo Demartino)

constructions. Currently, glued laminated bamboo (glubam) stands as a premier engineered bamboo product for structural applications due to its notable strength and durability [1, 2, 3, 4]. However, despite its high strength, glubam is inherently brittle [2, 5], necessitating the use of ductile joints in its structural applications to accommodate movement and stress.

Bolted connections are fundamental to the structural integrity of wooden trusses and moment-resisting frames. Extensive research over the years has focused on analyzing the mechanical behaviors of these connections. In this field, the predominant research methods include experimental studies, which provide direct observations of behavior under various conditions, comprehensive three-dimensional (3D) finite element (FE) simulations that offer detailed insights into stress and strain distributions, and simplified phenomenological models that abstract and generalize the mechanical responses [6].

Experiments are the cornerstone of analyzing mechanical behaviors, providing essential data that form the foundation for understanding the hysteretic properties of structures. The structural performance of bamboo- and timber-based structures is primarily governed by the nonlinear response at the connection zones, where significant deformation and stress concentrations occur around fasteners such as rivets, nails, dowels, or bolts. Consequently, exploring the nonlinear behavior of bolted glubam connections, particularly under conditions of extensive deformation leading to failure, is crucial for understanding and improving the resilience of these structures. In this context, Stehn and Börjes [7] investigated the influence of ductile slotted-in nailed wood on steel joints regarding the overall load-carrying capacity and deformability of a glulam truss. Shu et al. [8] and He et al. [9] used bolted glulam connections with a slotted-in steel plate as knee braces for glulam beam-to-column connections and ascertained its moment resisting performance. Leng et al. [10] studied the moment-rotation behavior of three types of different beam-to-column bolted connections in bamboo scrimber structures. Shu et al. [11] proposed innovative moment-resisting connections for mid-rise timber moment frame structural systems. These connections are reinforced by using long steel rods with screw-heads and long self-tapping screws, thereby providing a stiff and resilient beam-to-column connection.

More specifically, existing research on modeling the mechanical behavior of timber joints or connections generally follows two approaches: (*i*) explicit modeling of all joint components, including timber, steel dowels, and other types of connectors [e.g., 12, 13]. This method allows for detailed predictions based on material properties and joint geometry, with the finite element (FE) model clearly illustrating the interactions between components. However, the complexity and scale of such models often result in high computational costs and convergence issues, making this approach most suitable for analysis at the structural member level. (*ii*) Alternatively, joints can be modeled as a whole using a single representative element with user-defined mechanical properties [e.g., 14, 15, 16]. Although this method simplifies the programming of user-subroutines and facilitates both member- and structural-level analyses, it also introduces complexity and potential convergence difficulties. Due to these challenges, there is a notable gap in the availability of

FE modeling approaches that are both easy to implement in commercial FE packages and applicable to structural-level analysis.

However, to construct a more robust and accurate FE model, a model updating process is necessary [17, 18, 19, 20, 21]. Numerical model updating can be defined as the process of calibrating a numerical model to minimize the discrepancy between the numerically predicted and measured responses of real structures [22]. The model updating process requires for advanced algorithms capable of working for large dimensional problems.

In the field of the model update of cyclic constitutive laws, Do and Ohsaki [23] addressed the challenge of accurately modeling the cyclic elasto-plastic behavior of structural steels subjected to earthquake excitation. They proposed using Bayesian optimization to efficiently infer the parameters of a combined isotropic/kinematic hardening model, based on experimental cyclic responses. The results demonstrate the robustness and effectiveness of Bayesian optimization in capturing the behavior of structural steels under different cyclic loadings, highlighting its potential for parameter identification in the absence of extensive material testing. Sessa et al. [24] presented an inverse strategy for parameter identification of a hysteretic constitutive model, allowing the closed-form expression of stress-strain or load-displacement relationships without iterative algorithms. Pelliciari et al. [25] delves into a crucial aspect of structural engineering: the identification of parameters for a modified Bouc–Wen model tailored to capture the behavior of degrading and pinched hysteretic systems more accurately. The parameter identification process itself is carried out using a Genetic Algorithm (GA), an optimization technique that efficiently searches for the best set of parameters by mimicking the process of natural selection. The GA is applied to force–displacement data obtained from experimental tests on physically modeled reinforced concrete bridge piers. By adjusting the model parameters to best fit the experimental data, the modified Bouc–Wen model demonstrates a high degree of accuracy in predicting the complex behaviors characteristic of structural degradation under load.

The traditional numerical model updating framework facilitates the adjustment of unknown model parameters [26, 27, 28]. However, these conventional approaches often struggle with the highly non-linear and non-convex optimization challenges presented in complex structural models. Such complexities can lead to excessive computational demands and, occasionally, results that do not meet the desired accuracy and efficiency standards.

To overcome these issues, this study introduces a refined model updating framework that integrates advanced algorithms designed to efficiently navigate the complicated optimization landscape. This innovative approach substantially lowers computational costs and enhances the accuracy and reliability of the model predictions. By leveraging parallel processing and genetic algorithms, the framework adeptly manages the large dimensionality of the problem, optimizing parameter estimation and offering a more robust solution for the dynamic analysis of bamboo- and timber-based structures, where non-linear responses are critical.

This research is motivated by the urgent need to bridge this knowledge gap and enhance the application

of glubam in structural engineering. By focusing on the axial and hysteretic behavior of steel to glubam connections, this study aims to provide a detailed analysis of their mechanical responses under various stress conditions, contributing significantly to the optimization of bamboo-based construction technologies. The objectives of this study are twofold: firstly, to experimentally investigate the mechanical properties of riveted and bolted glubam connections, and secondly, to develop and validate a sophisticated finite element model that accurately predicts the behavior of these connections under load. The results derived from this research are expected to guide the design of more resilient and efficient bamboo-based structures, paving the way for broader adoption in the construction industry.

This study begins with an experimental investigation of the axial behavior of bolted steel to glubam connections, specifically focusing on their hysteretic response. We conducted axial hysteretic tests on connections integrated within roof truss structures, examining four distinct configurations corresponding to four different roof trusses. Following the experimental phase, we employed numerical simulation methods to perform nonlinear time-history analysis on both truss joints and the overall roof truss systems.

To address the computational challenges on the FE modelling of the hysteretic behaviour, this paper introduces a novel, computationally efficient nonlinear numerical model in ABAQUS that accounts for the hysteretic behavior of individual joints by integrating multi-axial connector and spring elements either in series or in parallel. These elements are assigned various constitutive laws to accurately simulate behaviors such as sliding, elasticity, plasticity, and pinching. Given the model's complexity and the necessity to accommodate a wide range of behavioral parameters, we propose the use of parallel genetic algorithms (PGA) to facilitate automatic parameter calibration. This framework minimizes the error between the predicted and tested hysteretic behaviors by linking the PGA optimization routines, implemented in Python, with the ABAQUS-Python interactive platform.

Building upon the calibrated parameters of the truss connections, we developed a simplified roof truss model in ABAQUS. This model combines the previously described multi-axial connector and spring elements (representing truss joints) with wire elements (representing truss chords), thereby providing a robust simulation tool for analyzing the structural dynamics of roof trusses under various loading conditions.

After this introduction, this paper is organized into six sections. Section 2 describes the materials and design specifications used in constructing the hybrid roof trusses, focusing on the innovative aspects of joint configurations and the choice of bio-based laminated materials. Section 3 outlines the test configurations employed to assess the structural integrity and performance of both truss joints and full truss assemblies under various loading conditions. In Section 4, we present the results of these tests, providing a detailed analysis of the mechanical behaviors observed and the implications for design and construction practices. Section 5 delves into the numerical investigation, where we describe the development and calibration of a sophisticated finite element model in ABAQUS, enhanced through the use of parallel genetic algorithms for parameter optimization and model updating. The conclusions of this research are summarized in Section

6, highlighting the key findings, the scientific and practical contributions to the field of civil engineering, and potential directions for future research. Appendices provide supplementary information including a flowchart of the parallel algorithm used in the model identification process (Appendix A) and the detailed framework of the identification strategy (Appendix B).

2. Hybrid planar roof truss: Materials, Design, and Construction

2.1. Details of joints

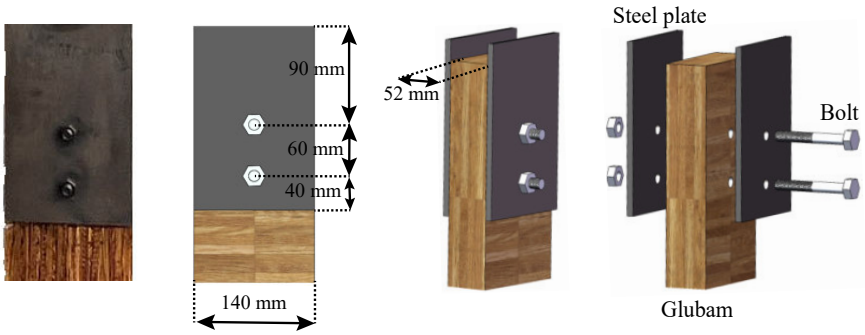

Figure 1: Detailed geometry of bolted steel to glubam joints.

Existing research on the use of a timber truss indicates that the joint region significantly influences the overall performance of truss structures [29]. The optimal design of joints can effectively improve the overall performance of truss structures [30, 31]. Therefore, in this study four different configurations of truss joints that adopting different diameters of bolt (10, 12, 14 and 16 mm) as shown in Table 1, were considered. The joints were named by following the designation B-A-J, where A is bolt diameters and B refers to bolted and J refers to joints.

Details regarding the geometry of the joints are presented in Figure 1. The truss elements sandwiched with two steel plates are composed of the glubam panel, Grade 8.8 bolts, and Q235 steel plates. All the joints were designed following the geometric requirements of GB50005 [32]. Holes were drilled on Glubam components and steel plates, and bolt inserted in these tight-fitting holes were adopted to connect the steel plates with Glubam components in ends of joined members.

Table 1: Configuration of designed joints.

Configuration	B-10-J	B-12-J	B-14-J	B-16-J
Diameter of bolt	10 mm	12 mm	14 mm	16 mm

2.2. Hybrid roof trusses

A total of four hybrid roof trusses were specially designed and assembled, corresponding to the four different configurations of truss joints mentioned above. Each roof truss consists of nine members with a span of about 4 m. The detailed geometry of the planar truss is presented in Figure 2. All the members were connected by using bolted steel to glubam connections. The shape of each steel plate was adapted depending on the specific number of branches at the considered node. Detailed shapes of the steel plates are also presented in Figure 2. All the truss members were manufactured using a CNC drilling machine. During the manufacturing process, the glubam bars were initially cut to specified lengths. Subsequently, two holes were precisely drilled at the both ends of each bar. Finally, to facilitate loading test, 50 mm diameter holes were drilled on the end steel plates of the lower chord and the middle steel plate of the upper chord to insert hinge pins. These hinge pins establish connections between the truss and the hinge supports or the loading actuator, respectively.

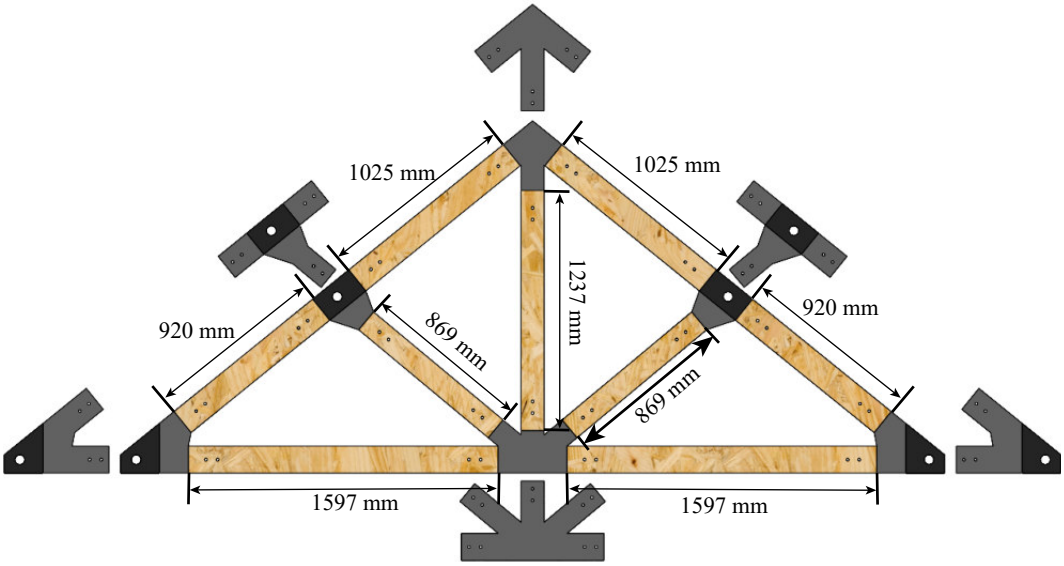

Figure 2: Detailed geometry of the roof truss.

3. Test configurations

3.1. Test on truss joints

A series of axial cyclic tests on the four different joints were conducted to obtain mechanical information of the joints. A sketch of the experimental setup is shown in Figure 3a. The hydraulic actuator installed vertically on the steel frame was utilized to apply the loading force through the predefined displacement. Because the hydraulic actuator was controlled by the computer, the actual displacement displays a difference from the predefined displacement shown by the computer. To solve this problem, a displacement transducer

(linear variable differential transformer (LVDT)) is attached to the surface of the connections. Control of the actuator is conducted based on the slip between the upper steel plate and the glubam components, as recorded by the displacement transducer.

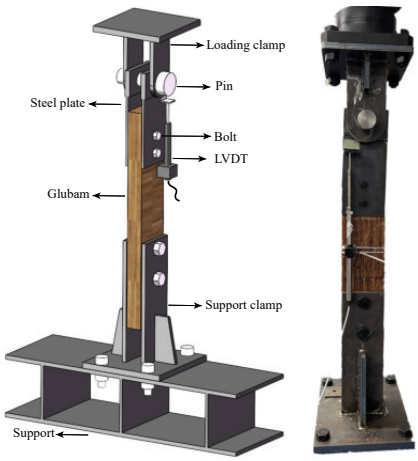

Figure 3: Test setup and instruments for joints test.

The cyclic loading protocol was conducted under displacement control, with a loading rate of 0.2 mm/s until failure (failure modes are discussed in the following sections) according to EN12512 [33]. The joints specimens were named according to Table 1.

3.2. Test on the roof truss

To validate the predicted hysteretic behavior stemming from the numerical model, cyclic tests were conducted on a series of full-scale roof trusses to obtain a hysteretic curve. The experimental setup for the planar truss is displayed in Figure 4. In this test, the end connections of the truss were joined to two steel supports that were in turn attached to the foundation using hinge pins, as shown in Figure 4. Two other hinge pins were inserted into the middle steel plates that were situated between the upper chords to establish a connection with the hydraulic actuator. This actuator was installed vertically on a reaction frame, thus enabling the application of the load. The vertical load was applied as a displacement history.

It should be noted that this study seeks to analyze the uniaxial behavior of truss structures and joints. Consequently, it is crucial to ensure that all truss elements experience only axial compression or tension

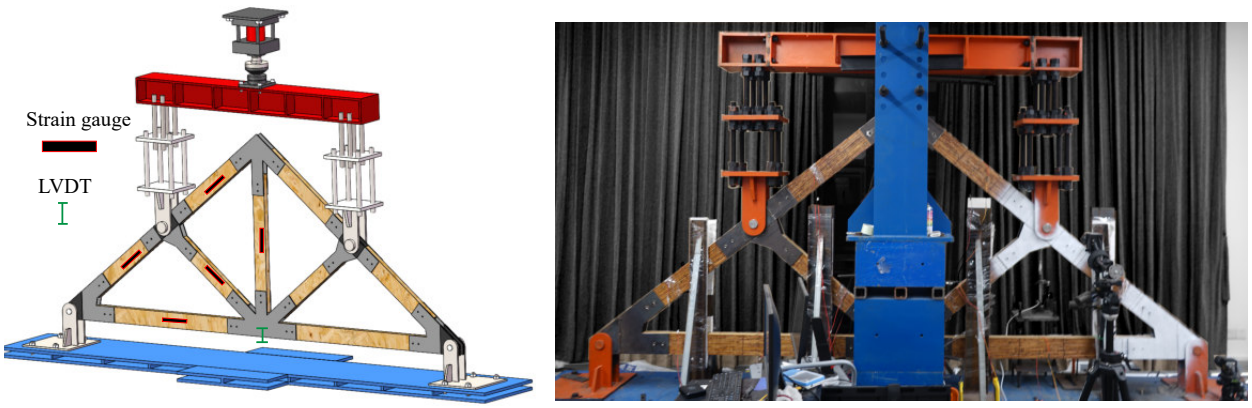

Figure 4: Sketch and photo of glubam roof truss test setup.

during the loading process. A lateral bracing system was applied herein to effectively constrain out-of-plane deformation. Several steel plates and braces are installed to prevent the deformation in the perpendicular direction, which can be regarded as rigid constraints. Therefore, only the constitutive law along the axial direction (parallel to the truss chord) is considered.

Strain gauges were utilized to measure the strains of the truss elements accurately. The layout of the strain gauge is presented in Figure 4. Considering the symmetry of the structure, measurements were taken on only half of the truss elements. Strain gauges were arranged on both sides of a single element to detect whether the moment existed inside each bar. The cyclic loading protocol was conducted under displacement control at a loading rate of 0.2 mm/s according to EN12512 [33].

The tested planar trusses were named by following the designation A-RT, where A is bolt diameters and RT refers to roof truss.

4. Test results

4.1. Test results of truss joints

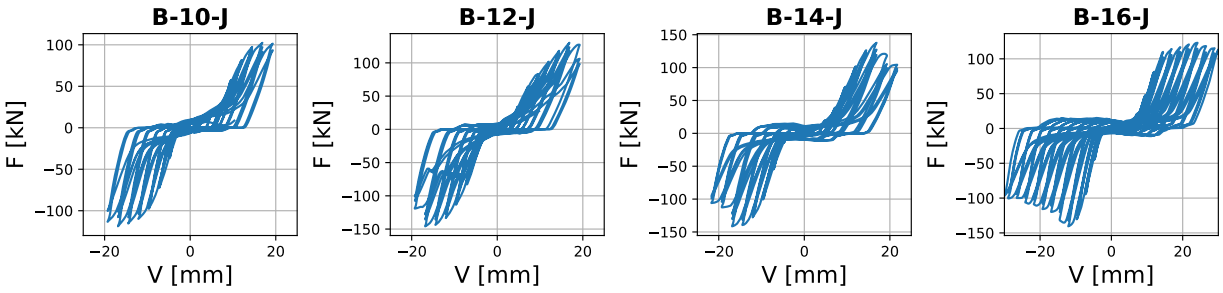

Figure 5: Load versus displacement curves obtained from roof truss joint tests under cyclic loading.

Figure 5 displays the hysteresis curves obtained from the cyclic loading tests conducted on the four different types of truss joints. The loading process covers the initial slip, elastic phase, yielding phase, loading plateau, and failure. Generally, the designed joints performed ductile behavior and their ductility increased with increasing diameter of bolt. The capacity increased with increasing diameters of bolt as well. As shown in Figure 6, joints will perform 3 types of failure pattern including fracture of bolt, shearing fracture of bolt head and shearing failure of glubam part between two bolts. Specimen B-10-J mainly shows the first two failure modes, while B-12-J, B-14-J, B-16-J mainly performed the last failure mode.

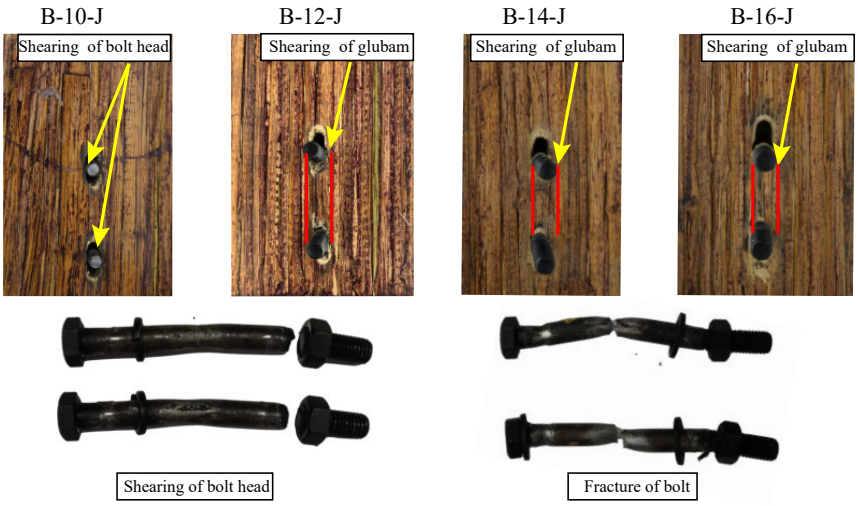

Figure 6: Failure patterns of joints.

4.2. Test results of roof truss

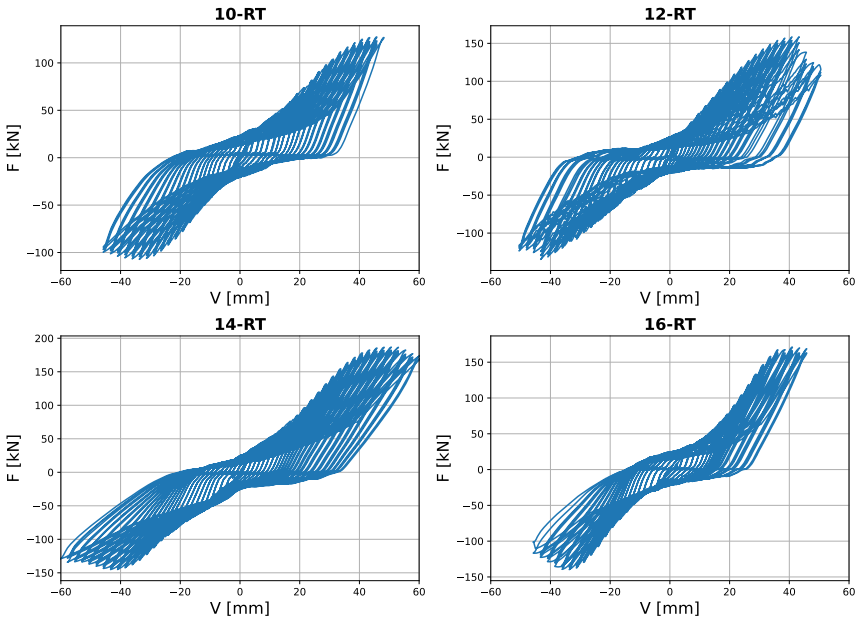

Figure 7: Load versus displacement curves obtained from planar roof truss tests under cyclic loading.

The hysteresis curves of four groups of planar roof trusses under cyclic loading are presented in Figure 7. The planar roof truss displayed similar hysteresis responses with a truss joint. However, the hysteresis curves of the planar truss exhibited a more obvious initial slip stage, especially on the compressive loading side. This could be attributed to the tolerance observed between the steel support and the hinge pin and the out-of-plane movement seen under the influence of compressive loading. The typical failure patterns of the tested roof trusses are shown in Figure 8. The failures of nearly all specimens originated from the upper truss chord, the one connected with support, and the two end joints at this chord either failed due to fracture of bolt or shearing of bolt head. This phenomenon was in good agreement with the stress status of each bar. Generally, the planar roof truss showed similar failure pattern with single joints test. Roof truss 10-RT showed the lowest capacity, while roof truss 12-RT, 14-RT and 16-RT showed larger capacity than 10-RT and their capacity are almost similar. This is because roof truss 10-RT failed earlier due to failure of bolt, while shearing of glubam is the major failure pattern for roof truss 12-RT, 14-RT and 16-RT, thus the capacity of which are only related to the shearing capacity of glubam.

5. Numerical investigation

5.1. Simplified model for truss joints in ABAQUS

To achieve a balance between model prediction accuracy and computational burden, a simplified and versatile phenomenological model that specify the envelope path and associated hysteresis is proposed in

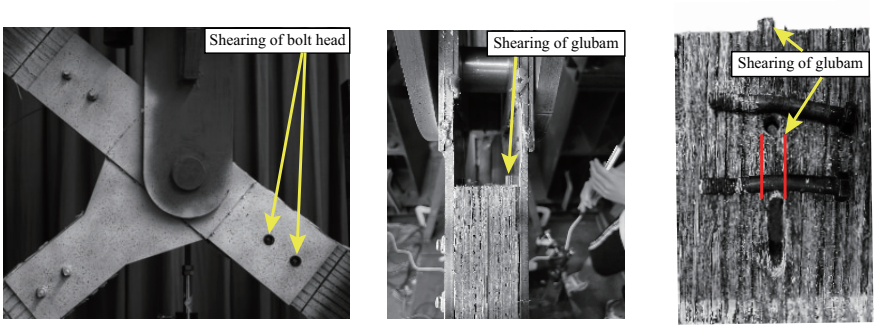

Figure 8: Typical failure pattern of planar roof trusses.

this study. The simplified modelling method used in this study is inspired by the methodology provided in [12] which involves combining a series of connector elements from which the hysteresis behaviour of the joints is generated.More specifically, the truss joint is modelled by a series of two-dimensional axial connector elements which are available in ABAQUS as CONN2D2. Basic behaviours are assigned to each element, namely, elasto-plastic behaviour (herein EP elements), STOP behaviour (herein S elements) and LOCK behaviour (herein L elements). In the present joint model, the positions of all nodes locate at the same position and mechanical behaviours are assigned to the tension and compression degree of freedom (DOF) of the connector elements only. Therefore, the plot of the FE mesh is a series of nodes positioned at the same location. In order to provide a more intuitive illustration, the tension and compression DOF of the elements are transformed to one dimensional translation. The connector elements are illustrated in Figure 9 while the joint model is shown schematically in Figure 10.

5.1.1. Behavior of connector elements

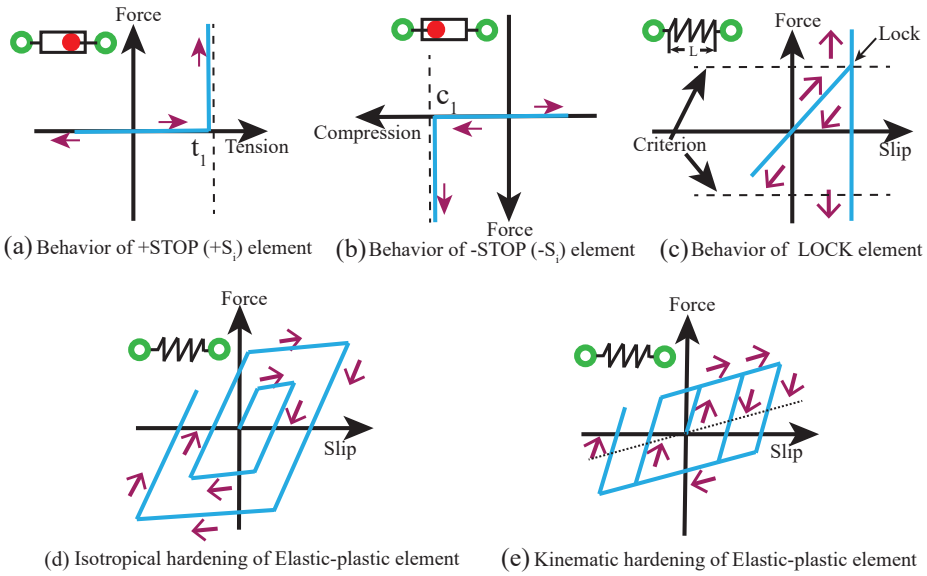

Figure 9: Behavior of connector elements.

In the model reported herein, elasto-plastic elements with one DOF are utilised as only uniaxial behaviour needs to be considered. As a result, there are four parameters that need to be defined for the EP element, namely (*i*) elastic stiffness, (*ii*) yield strength, (*iii*) post-yield stiffness, and (*iv*) hardening rule.

The hardening rules used within this study includes isotropic hardening and kinematic hardening. The rules are respectively shown in Figure 9 d and e. The isotropic hardening rule specifies that the centre of the yield surface remains at its original position and that the yield surface expands with positive post-yield stiffness. The kinematic hardening rule specifies that the shape of the yield surface remains the same and that the centre of the yield surface moves with the yield stress.

The behaviour of the S elements can be described as a slider positioned in a slot that has a finite length. This type of element contains two nodes (i.e., one node is the slider, and the second node is the slot) as provided in Figure 9 (a) and (b). The minimum and maximum deformation is limited by the two boundaries of the slot node, while deformation of the element occurs without friction within the limit of the two boundaries.

The behaviour of an L element is shown in Figure 9 (c). The element is assigned a threshold value which is expressed in terms of either deformation or internal force. Before the threshold value is achieved though, the element behaves according to the original properties that are assigned to it. The element will be "locked "and defined as a rigid body when it achieves the threshold value. In this case, the distance between the two nodes will no longer change. Finally, the L element is defined by linear-elastic behaviour with internal force as the threshold criterion.

5.1.2. Proposed joint model

The physical mechanisms contributing to the pinched-style hysteresis behaviour of the bolt-type timber joints are comprised of four basic stages.

1. Loading: The bolts are in contact with the glubam hole (i.e., a hole that accommodates a steel bolt), the glubam is subjected to bearing load and the bolts are subjected to bending. In this stage, the bolts and timber work together to resist the external load.
2. Unloading: The bolts separate from the bearing wall of the hole and slide in the deformed hole. In this stage, friction force is the dominant action resisting the applied load.
3. Reloading/reverse loading: The bolts are bent in an opposing manner and slide in the deformed hole until they fully contact with the wall of the hole.
4. Strength degradation stage: The glubam exhibts shear crack as the bolt continue to embed.

Based on these physical interpretations, a model is proposed in this paper that is informed from four key assumptions: (*i*) EP elements are used in conjunction with slot elements in order to represent the bearing of glubam as well as the permanent deformation of the hole; (*ii*) friction force and reverse bending of the bolts are all considered in the steel bolt model; (*iii*) three groups of EP + S elements are connected in parallel in order to achieve yield of the glubam representing contact between the bolts and glubam hole in the reloading/reverse loading stage; (*iv*) The EP element is incorporated with damage behaviour representing strength degradation due to shearing failure of glubam. Details of the model formulation are now further elaborated upon.

As indicated at the beginning of this section, the contributions of the steel bolt, glubam bearing are modelled individually while the overall behaviour of the joint involves the superposition of the actions contributed by all components. Figure 10 provides key details about the joint model. The overall model is shown schematically in Figure 10 (a). In addition, the combinations of connectors shown in Figure 10 (b) and (d) represents the behaviour of the steel bolt action and glubam bearing action, respectively, while their monotonic force-slip behaviours are plotted schematically in Figure 10 (c) and (e), respectively. According to the assumptions of superposition, the capacity of the joint is given by:

$$F(V) = F_s(V) + F_b(V) \tag{1}$$

where F is the joint force, F_s is the force contributed by the steel bolt model, F_b is the force contributed by the glubam bearing model, and V is the slip of the joint. Details of these three models are provided in the following sections.

Bolt model. The behaviour of the steel bolt is modelled by connecting an EP element, an L element and a S element in series (see Figure 10 (b)). The L criterion is set to be equal to the yield strength of the

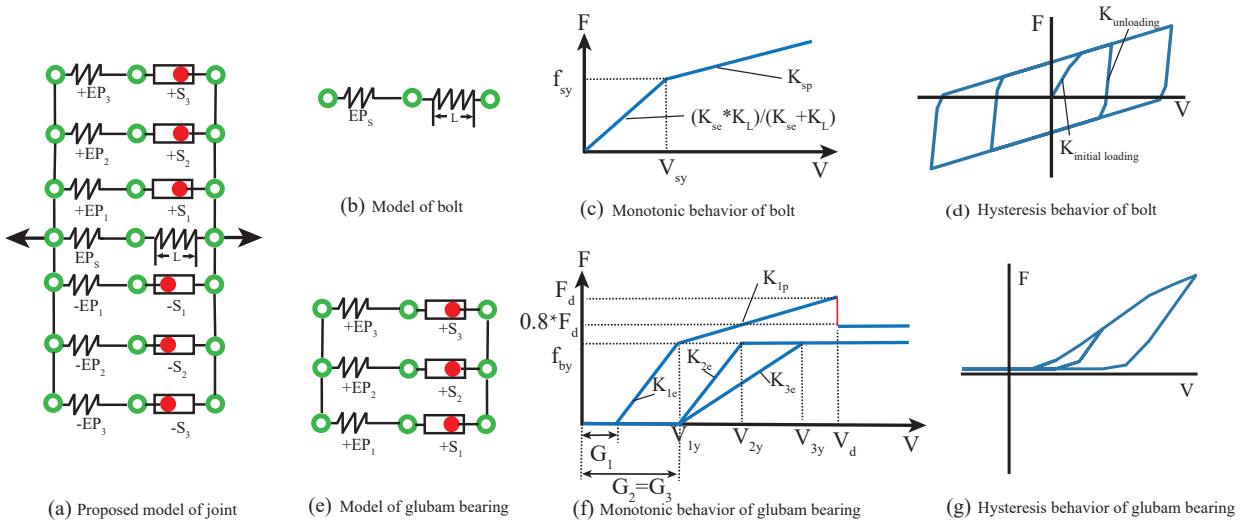

Figure 10: Model of the hysteresis behaviour of truss joints.

EP_s element. The elastic stiffness obtained by the steel bolt model can therefore vary before and after yielding of the bolt, thus simulating the embedding process of the bolts with a lower initial stiffness before yielding. The S elements model a one-sided constraint of the joint as shown in Figure 10. For $+S_i$, when it is combined with other elements in series, it can model the initial sliding behavior caused by the tolerance between bolt and bolt hole. Here, the distance between the slider and the right end of the slot (upper limit) is set to be equal to the real manufacture tolerance, G_1. Based on the definition of $+S_1$, the EP and LOCK element connected to it can only achieve a net positive load under positive deformation. Similarly, the EP and LOCK element connected to $-S_i$ can only achieve a net negative load under negative deformation. It is proposed that the plasticity of the steel bolt (EP_s) is defined by kinematic hardening. The force that is contributed by the steel bolt under monotonic loading can therefore be calculated using:

$$F_s\left(V\right) = 0\left(V < G_1\right) \tag{2a}$$

$$F_s\left(V\right) = K_{se}K_L/\left(K_{se}+K_L\right)\cdot V\left(G_1 < V < V_{sy}\right) \tag{2b}$$

$$F_s\left(V\right) = K_{sp}\left(V - V_{sy}\right) + f_{sy}\left(V \geq V_{sy}\right) \tag{2c}$$

Glubam bearing model. A combination of EP and S elements is used to model the bearing of glubam, as shown in Figure 10. As mentioned above, The S elements also model a one-sided constraint of the joint. Here, the distance between the slider and the right end of the slot (upper limit) is set to be equal to the gap width, $G_i\,(i = 1, 2, 3)$. The distance to the left end (lower limit) of the slot is set to be a large value which

is impossible to reach (i.e., 30 mm). Details about the irrecoverable deformation of glubam and the contact status between the steel bolt and the glubam are retained by the S element.

Several assumptions are made for the glubam bearing action model, namely (i) the yield strengths for EP_1, EP_2 and EP_3 are equal, (ii) EP_2 and EP_3 are elasto-perfect plastic, and (iii) the hardening rule for EP_i ($i = 1, 2, 3$) is delineated by isotropic hardening. With these assumptions, a gradual elasto-plastic transition stage of the force-slip curve can be achieved, and the loading and unloading stiffnesses can be set unequal to each other. Based on the model and assumptions described above, the resistance force generated by the glubam bearing action can be calculated using the following equations:

$$F_b\left(V\right) = \Sigma F_i\left(V\right) \qquad (i = 1, 2, 3) \tag{3a}$$

$$F_i\left(V\right) = 0 \qquad (V < G_i) \tag{3b}$$

$$F_i\left(V\right) = K_{ie}\left(V - G_i\right) \qquad G_i < V < V_{iy} \tag{3c}$$

$$F_i\left(V\right) = K_{ip}\left(V - V_{iy}\right) + f_{by} \qquad V_{iy} < V < V_d \tag{3d}$$

$$F_i\left(V\right) = K_{id}(V - V_d) + 0.8 * F_d \qquad V > V_d \tag{3e}$$

where F_i is the force generated by the i th glubam model, G_i is the gap of the S_i element, V_{iy} is the yield displacement of the i th glubam model, K_{ie} is the elastic stiffness of the EP_i element, K_{ip} is the post-yield stiffness of the EP_i element ($K_{2p} = K_{3p} = 0$), and f_{by} is the yield strength of the EP_i element, F_d is the load of the EP_i element immediately after it is damaged, while V_d is the damage initiation displacement. In this study, only EP_1 element is considered with damage behavior to simulate the loading descending stage.

Asymmetric behavior of glubam bearing model. The gluabm exhibit asymmetric bearing behavior at the tension and compression direction, thus 3 $+EP$ element combined with $+S$ element are adopted to model the positive hysteretic behavior of glubam bearing, while 3 $-EP$ element combined with $-S$ element are adopted to model the negative hysteretic behavior of glubam bearing.

5.2. Initial parameter identification of truss joint model

The proposed model holds a large number of flexible parameters. Hence, automatic parameter calibration is indispensable. This paper presents a novel parallel genetic algorithms (PGA) based framework aimed at identifying parameters to minimize force-time history error between predicted hysteretic behavior from simplified joints model and tested behavior.

5.2.1. Parallel genetic algorithms (PGA) and parallel computing system

Genetic algorithms (GA) are a discrete evolution strategy method which employs an iterative procedure on the basis of evolution of a design population over a selected number of generations [34, 35]. In each iteration of this procedure, the design population is first evaluated in conjunction with response and constraint function calculations performed for each design, and then a sequential application of the recombination, mutation and selection operators takes place to constitute the individuals of the next generation. GA are very suitable for many problems, but often require too much time and therefore may be disadvantageous. The most time-consuming operation within GA is the evaluation of the fitness function [36, 37]. Hence, an effective and adequate parallelization of the solution algorithm can be accomplished by creating multitasked regions in the GA source code for this step only, since fitness evaluation of the design population does not entail any inter-processor communication, and thus can be conducted concurrently by a number of threads in a parallel computing environment.

The serial algorithm is organized in a number of sequential and parallel code segments to achieve a master-slave configuration based parallel programming structure. The sequential code segments (recombination, mutation and selection) are only accessible by the master thread, whereas multitasked loops (numerical simulation calculation and fitness evaluation) encapsulated in parallel codes are executed by slave threads. Additional sequential code segments are written for enabling coordination, communication and synchronization within the network by the master thread.

The parallel execution of the solution algorithm is schematically depicted in Figure A.23 in Appendix A. Accordingly, once the algorithm is initiated, the input data describing the aforementioned parametric model (Inp file) is first distributed to all the slave threads by the master. Then, the initial population that, in the current case, represent different constitutive parameters of material model, is generated by the master thread based on a random initialization of parameters to be identified. Next, the master calls all the slave threads to perform evaluation of the design population collectively and concurrently. Each design (parametric model) is assigned to each slave thread within the parallel computing system by the master. Every thread undertakes numerical simulation response calculations, response output and fitness evaluation calculations for the subset of designs assigned to itself in conjunction with ABAQUS platform. The results of analyses and evaluations are reflected in single numerical values, which are delivered from slave thread to the master as the objective function scores of the individuals. The master thread waits until every thread in the parallel computing system completes its own task. It then continues to implement evolutionary operators in a sequential manner to yield the design population of the next generation, while slave threads are put on hold in the meantime until response and fitness evaluation calculations are processed in the next generation.

5.2.2. Rough estimation of parameters

Preassigning values of certain parameters and defining a restricted searching space for parameters to be optimized (e.g. limiting the optimization to a portion of parameters instead of the whole) can dramatically reduce the computational cost of the calibration. Thus, it is critical to perform a rough estimation of parameters first, which involves extraction of the characteristic points and parameters of the hysteresis curves from the tested results (i.e., the stiffness, K, and the yield slip, V_y). The definition of characteristic points and the rough determination of model parameters will be introduced in this section.

Herein, only the model parameters controlling the hysteresis curve at the positive side is discussed and parameters describing the negative side can be deduced in the same way. To solve all the unknown parameters controlling the hysteresis curve at the positive side, the initial stiffness, K, yield slip, V_y and four characteristic points, P_1 , P_2 , P_3 , P_4, and P_5 on the hysteresis curves at the positive side are needed to be specified additionally, as shown in Figure 11.

$P_1(V_1, F_1)$ and $P_2(V_2, F_2)$ are determined as the hardening-initiating point and peak-loading point respectively, which could be roughly estimated from the hardening segment of the hysteretic curve. $P_3(V_3, F_3)$ are determined as the damaged point corresponding to a load equal to 80% of maximum force. $P_4(V_s, 0)$ are determined as the intercept of the hysteresis curve on the $+x$ axis and $P_5(0, -f_s)$ as the intercept of the hysteresis curve on the $-y$ axis, both of which could be roughly estimated from the unloading segment. Since more stable curves will result from repeated load cycles, it is suggested to define P_4 and P_5 in the last cycle.

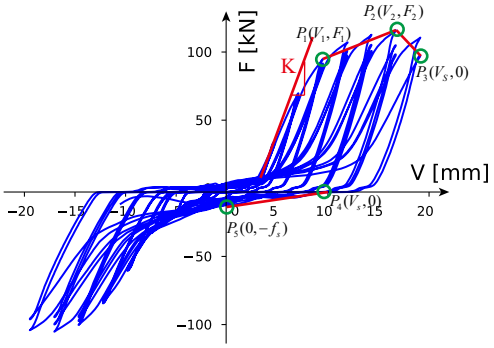

Figure 11: Selection of characteristic points on hysteresis curves for simplified model development.

The proposed method for roughly determining the parameters is defined by several steps, namely, (i) the initial stiffness of the model $= K$, (ii) the yielding of the steel bolt model $= V_y$, (iii) the post-peak stiffness of the steel bolt model = the slope of the line P_4-P_3, (iv) the yield strength of the steel bolt model $= f_s$, and (v) the moment of the model is equal to that of the test results at $V = V_1$ and $V = V_2$. Additionally, it is proposed $G_2 = G_3 = G_1 + f_{by}/K_{1e}$,$V_{2y} = 0.5(V_1 + V_y)$ and $V_{3y} = V_1$, where V_y is the yield rotation of the joint adopted from the test results. With these assumptions, the EP_2 and EP_3 elements can begin

to work instantaneously after EP_1 yields, while the contribution of the glubam bearing increases linearly according to slope K_{1p} when the slip of the joint is greater than V_1. Yield of EP_2 and EP_3 can simulate the transition from the elastic stage to the post-yield stage.

Based on the conditions listed above, the following equations must therefore be satisfied:

$$\begin{aligned} K_{se}K_L/(K_{se}+K_L)+K_{1e} &= K \\ V_{sy} &= V_y \\ K_{sp} &= f_s/(V_s) \\ f_{sy} &= f_s \\ F\left(V_1\right) &= F_1 \\ F\left(V_2\right) &= F_2 \\ F\left(V_3\right) &= F_3 \end{aligned} \tag{4}$$

By substituting Eqs. 1, 2b and 2c into Eq. 4, the parameters of the steel bolt and glubam bearing models can be calculated. For the bolt model:

$$\begin{aligned} f_{sy} &= f_s \\ K_{sp} &= f_s/(V_s) \\ K_L &= \tfrac{f_{sy}K_{se}}{K_{se}V_y-f_{sy}} \end{aligned} \tag{5}$$

For the glubam bearing model:

$$\begin{aligned} K_{1e} &= K-f_{sy}/V_y \\ K_{1p} &= \tfrac{F_2-F_1}{V_2-V_1}-K_{sp} \\ f_{by} &= \tfrac{F_2-f_{sy}-V_2(K_{1p}+K_{sp})+V_yK_{sp}+G_1K_{1p}}{3-K_{1p}/K_{1e}} \\ G_2 &= G_3 = f_{by}/K_{1e}+G_1 \\ K_{2e} &= \tfrac{f_{by}}{0.5(V_y+V_1)-G_2-G_1} \\ K_{3e} &= \tfrac{f_{by}}{V_1-G_2-G_1} \end{aligned} \tag{6}$$

It is observed from the hysteresis curves that the initial loading stiffness is always smaller than the unloading stiffness. The lock element in the steel dowel model is hence applied herein to model this phenomenon. Among the above equations, there are two indeterminate parameters, K_{se} and K_L, which can be solved by assuming one of the values. Through pilot parametric studies, when increasing the value of K_{se}, the arising unloading slope will be steeper although there is less effect on the dissipated energy. This observation was also noted in reference [14]. Therefore, the rough estimated values of K_{se} is assumed to be 35 kN/mm in order to achieve a best fit to the unloading stiffnesses.

5.2.3. Identification framework

The parameter calibration framework proposed herein is based on the above-mentioned Parallel genetic algorithms (PGA) and parallel computing system. The flowchart of this calibration framework is depicted in Figure B.24 in Appendix B.

The "Initial decision" allows preassigning values of certain parameters and defining a restricted searching space for parameters to be optimized. As it can be observed in Figure B.24 in Appendix B, the core of the framework is the identification algorithm. The algorithm involves the definition of a proper objective function that estimates the error between simulated force-time history from simplified model and tested force-time history:

$$OF\left(\boldsymbol{\theta}\right)=\frac{\int_{v_0}^{v_f}\left|\left[\mathbf{F}_O\left(v\right)-\mathbf{F}_S\left(\boldsymbol{\theta},v\right)\right]\right|\mathrm{d}v}{\int_{v_0}^{v_f}\left|\mathbf{F}_O\left(v\right)\right|\mathrm{d}v} \tag{7}$$

where $\boldsymbol{\theta}$ is the vector collecting the model parameter to be identified:

$$\boldsymbol{\theta}=\left\{K_{1e}^{+},f_{by}^{+},K_{1p}^{+},K_{2e}^{+},K_{3e}^{+},G_1^{+},G_2^{+},K_{1e}^{-},f_{by}^{-},K_{1p}^{-},K_{2e}^{-},K_{3e}^{-},G_1^{-},G_2^{-},K_L,f_{sy},K_{se},K_{sp},F_d^{+},F_d^{-}\right\} \tag{8}$$

where v_0 and v_f are the initial and final displacement records, $\mathbf{F}_O\left(v\right)$ is the force derived from the tested data, and $\mathbf{F}_S\left(\boldsymbol{\theta},v\right)$ is the force simulated by the proposed simplified model. The values of $\mathbf{F}_S\left(\boldsymbol{\theta},v\right)$ is obtained by performing a cyclic analysis of proposed simplified model in ABAQUS platform in Python. Then the objective function value is mapped to fitness values and the fitness values of each tentative solution is evaluated. The fittest individuals are cyclically selected and recombined until the optimal parameters configuration are obtained.

Table 2: Rough estimation of parameters to be identified and the searching space.

Parameters	K_{1e}^{+} [$\frac{\text{kN}}{\text{mm}}$]	f_{by}^{+} [kN]	K_{1p}^{+} [$\frac{\text{kN}}{\text{mm}}$]	K_{2e}^{+} [$\frac{\text{kN}}{\text{mm}}$]	K_{3e}^{+} [$\frac{\text{kN}}{\text{mm}}$]	G_1^{+} [mm]	G_2^{+} [mm]	K_{1e}^{-} [$\frac{\text{kN}}{\text{mm}}$]	f_{by}^{-} [kN]	K_{1p}^{-} [$\frac{\text{kN}}{\text{mm}}$]	K_{2e}^{-} [$\frac{\text{kN}}{\text{mm}}$]	K_{3e}^{-} [$\frac{\text{kN}}{\text{mm}}$]	G_1^{-} [mm]	G_2^{-} [mm]	K_L [$\frac{\text{kN}}{\text{mm}}$]	f_{sy} [kN]	K_{se} [$\frac{\text{kN}}{\text{mm}}$]	K_{sp} [$\frac{\text{kN}}{\text{mm}}$]	F_d^{+} [kN]	F_d^{-} [kN]
B-10-J	8.4	12.19	4.5	2.4	2.2	1.5	1.45	8.4	15.21	4.5	2.93	2.7	1	1.81	1.9	8	20	0.6	70.5	92.3
B-12-J	11.5	15.52	5.5	2.33	2.13	1.5	1.35	11.5	18.51	5.5	3.14	2.9	1	1.61	1.7	10	25	0.8	90	114
B-14-J	13.6	6.05	8	0.6	0.4	1.5	0.44	13.6	4.4	8	0.62	0.7	1	0.32	1.6	12	30	1.1	118	132
B-16-J	15.67	21.09	2	1.89	1.6	1.5	1.35	15.67	35.76	2	3.3	2.9	1	2.27	1.5	11	35	1.2	91	70

Table 3: Setting of the PGA.

Pop.size	N.Generation	Evaluation	N.Slave threads	N.cores per thread
30	50	1500	30	1

5.2.4. Identification results

After rough determination of model parameters (see Section 5.2.2), for parameters that can be directly obtained from prior knowledge or experimental observations, such as G_i, we only multiplied the initial

estimated values as reported in Table 2 by amplification factors of 7 and 0.4, respectively, to serve as their upper and lower bounds in the search space. For other parameters, we multiplied the initial estimated values by amplification factors of 20 and 0.2, respectively, to serve as their upper and lower bounds in the search space. The population size and generation number are chosen as 30 and 50, thus, the identification process will perform a total of 1500 times evaluation, where 30 slave threads are arranged to evaluate 30 individuals simultaneously in each generation and 1 processors are distributed to execute each thread, as reported in Table3.

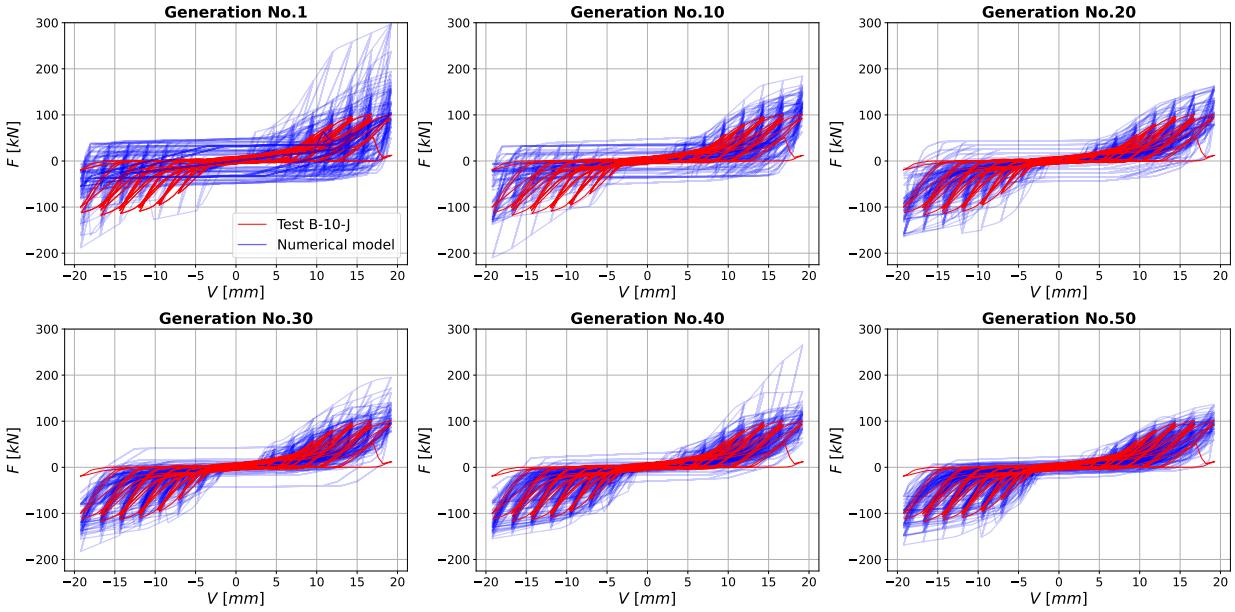

(a) B-10-J

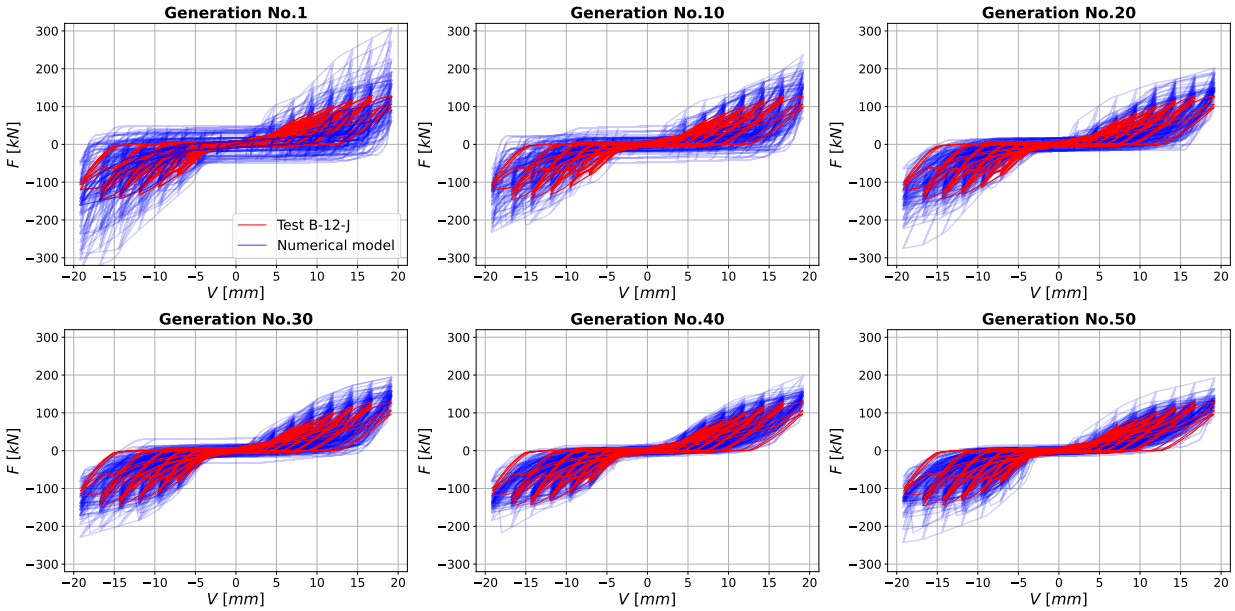

(b) B-12-J

Figure 12: Identification results over each individual in each generation: (a) B-10-J and (b) B-12-J.

Under the above settings, the identification process for the reference model has shown the convergence history illustrated in Figure 12 and 13. In particular, Figure 12 illustrated the identification results for B-10-J and B-12-J over each individual in some representative generations. It can be observed that the identification tends to a stable solution after about 30 generations, 900 evaluations of individuals and a

good agreement between predicted responses from proposed simplified model and benchmark response from test is achieved in the last generation.

This gradual optimization process can also be reflected in the moving trend diagram of the best objective function values as shown in Figure 13, where the objective function evaluations are reported according to Eq. 7. In the same diagram, the moving average trend is also reported. In Figure 13, the blue points indicate the best-performing individual or solution at each generation while the red points the average of the entire population's performance at each generation. The convergence of the blue and red points throughout the generations is particularly noteworthy. As the mean of the population converges towards the best solutions, it implies a reduction in the variability among the solutions in the population. This is indicative of the population stabilizing around more optimal solutions, which is a desired outcome in any optimization process. Such convergence signifies that the algorithm is effectively escaping local minima and making steady progress toward the global optimum.

The predicted hysteretic behaviors from the best individual after PGA identification for all the 4 cases are illustrated in Figure 12. It can be observed the proposed model can fit the pinching, damage and asymmetric behavior very well, and the energy dissipation also achieve a good fit between tested and predicted values. The final identified parameters for 4 cases are concluded in Table 4.

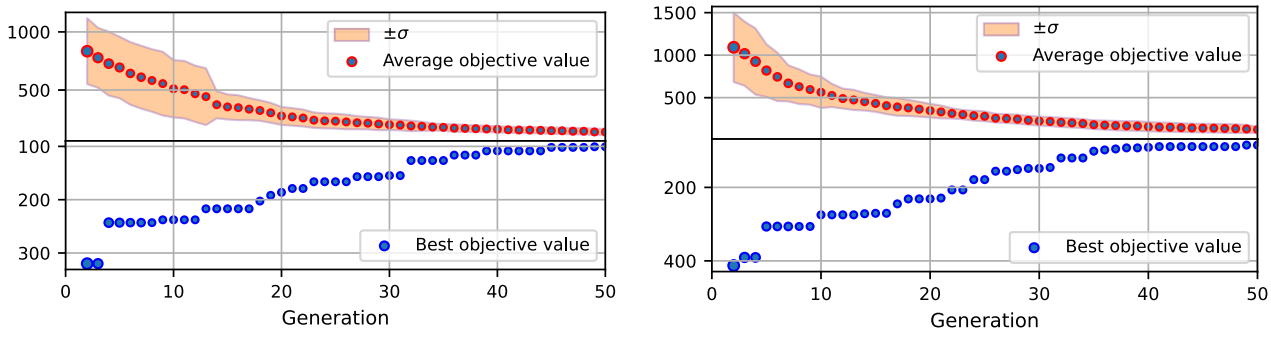

(a) B-10-J (b) B-12-J

Figure 13: Convergence history of the identification over the objective function evaluation: (a) B-10-J and (b) B-12-J.

Table 4: Identified parameters of simplified model for truss joints.

Parameters	K_{1e}^{+} [$\frac{kN}{mm}$]	f_{by}^{+} [kN]	K_{1p}^{+} [$\frac{kN}{mm}$]	K_{2e}^{+} [$\frac{kN}{mm}$]	K_{3e}^{+} [$\frac{kN}{mm}$]	G_1^{+} [mm]	G_2^{+} [mm]	K_{1e}^{-} [$\frac{kN}{mm}$]	f_{by}^{-} [kN]	K_{1p}^{-} [$\frac{kN}{mm}$]	K_{2e}^{-} [$\frac{kN}{mm}$]	K_{3e}^{-} [$\frac{kN}{mm}$]	G_1^{-} [mm]	G_2^{-} [mm]	K_L [$\frac{kN}{mm}$]	f_{sy} [kN]	K_{se} [$\frac{kN}{mm}$]	K_{sp} [$\frac{kN}{mm}$]	F_d^{+} [kN]	F_d^{-} [kN]
B-10-J	16.4	12.19	6.13	2.4	2.2	2.5	1.45	11.4	8.21	5.6	2.93	2.7	5.5	1.81	1.5	11.3	20.6	0.60	80.5	71.3
B-12-J	10.5	12.52	5.1	2.33	2.13	3.6	1.35	11.5	18.51	5.48	3.14	2.9	2.5	1.61	2.1	10.3	35.1	1.06	71.2	94.3
B-14-J	10.6	16.05	5.68	2.6	2.4	4.4	1.84	16.6	16.42	6.78	3.42	3.3	3.9	1.82	2.2	10.5	25.5	0.79	81.2	105.2
B-16-J	25.5	17.52	10.13	3.33	3.13	3.1	1.65	12.5	15.51	4.06	3.147	2.85	6.8	1.63	2.5	12	20.3	0.79	77.6	65.3

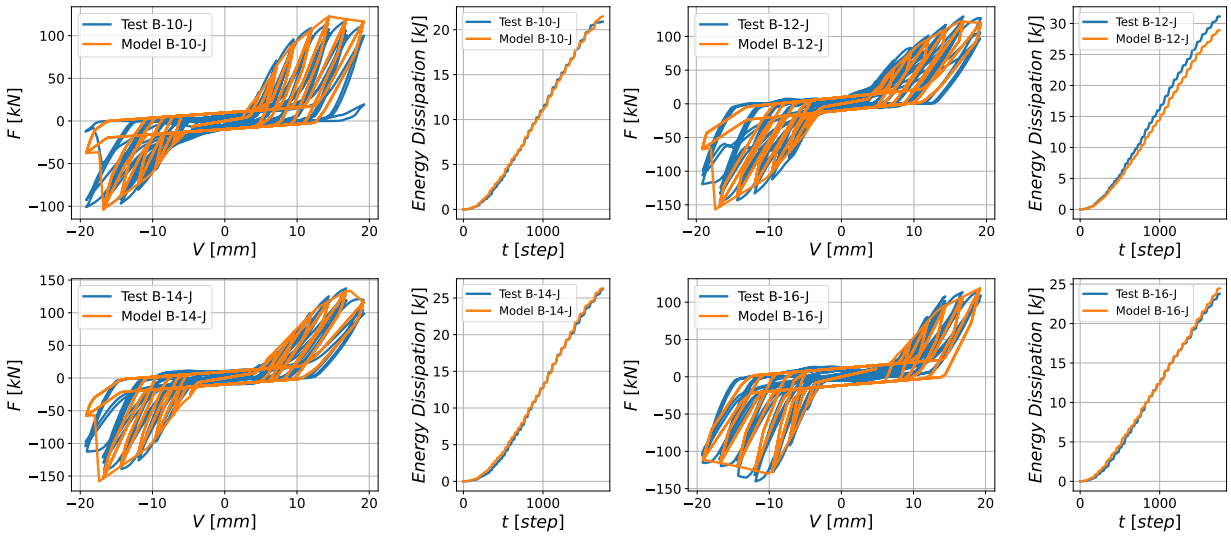

Figure 14: Comparison of tested hysteretic behavior and predicted hysteretic behavior from the best individual after PGA identification.

5.3. Model updating of hybrid roof truss

In last section, the key model parameters are preliminarily identified. However, it should be noted that this highly idealized structural model localizes the modeling of nonlinear behavior in a few prescribed elements, leading to potential model uncertainty. Moreover, the preliminary parameter identification is only carried out on individual joints level and the identification benchmark is only based on a single test, which itself has certain uncertainty. Therefore, To address this model uncertainty and construct more robust structural models with more accurate parameters, a PGA based model updating framework for the roof truss structures is proposed in this section.

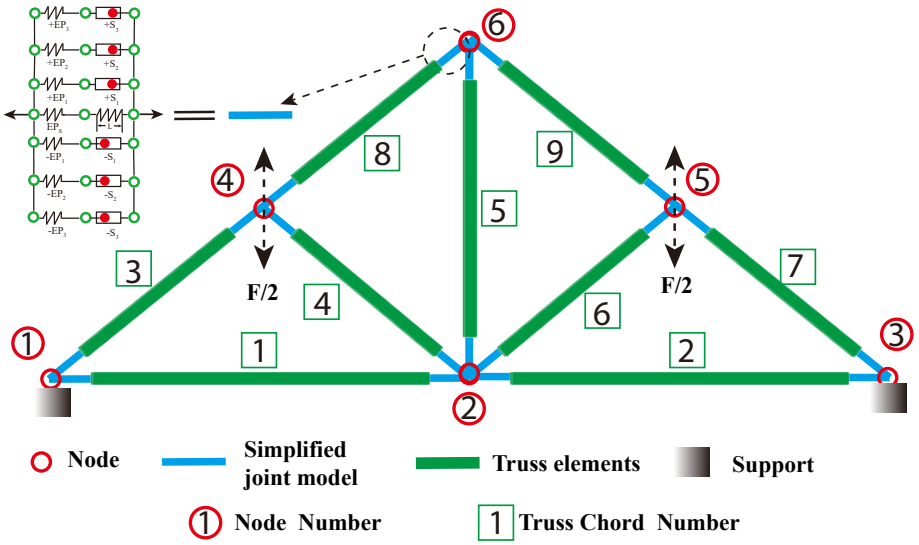

Figure 15: Simplified hybrid roof truss model in ABAQUS.

For this purpose, a simplified hybrid roof truss model is developed by combining the proposed joints model with wire element (truss chords) in ABAQUS as shown in Figure 15. The joint model is located between the node and wire element and its length is set as 150mm, which equals to the length of real joints domain (see Figure 1). The connector type used to connect the multiple axial connector elements with truss elements is translation type. Wire element is assigned with truss beam property, where the elastic modulus is 13 Gpa [38, 39] and section area is 140 mm × 52 mm. All the nodes are assumed as hinge connection and the support adopts pin connection, which complies with real boundary conditions. The benchmark of updating refers to cyclic test results of 4 hybrid roof trusses. The loading scenario of real hybrid roof truss is shown in Figure 4 and 15. A displacement-based cyclic loading is applied on node 4 and 5.

The updating framework is similar to identification framework with truss joints. The differences are the input parametric model and basic PGA setting. Considering truss model is more complicated than individual joint model, The iterative generation and population size is selected as 50 and 40, respectively, leading to a total of 2000 times evaluation, and 30 slave threads are assigned to undertake updating task. An amplification factor 5 and a reduction factor 0.5 assigned to initial parameter identification values of joints model are selected as the upper bound and lower bound of the searching space for hybrid truss updating.

5.3.1. *Model updating results*

Table 5: Identified parameter values from joints and updated parameters values from hybrid roof truss model.

Configurations	Parameters	K_{1e}^{+} [$\frac{kN}{mm}$]	f_{by}^{+} [kN]	K_{1p}^{+} [$\frac{kN}{mm}$]	K_{2e}^{+} [$\frac{kN}{mm}$]	K_{3e}^{+} [$\frac{kN}{mm}$]	G_{1}^{+} [mm]	G_{2}^{+} [mm]	K_{1e}^{-} [$\frac{kN}{mm}$]	f_{by}^{-} [kN]	K_{1p}^{-} [$\frac{kN}{mm}$]	K_{2e}^{-} [$\frac{kN}{mm}$]	K_{3e}^{-} [$\frac{kN}{mm}$]	G_{1}^{-} [mm]	G_{2}^{-} [mm]	K_{L} [$\frac{kN}{mm}$]	f_{sy} [kN]	K_{se} [$\frac{kN}{mm}$]	K_{sp} [$\frac{kN}{mm}$]	F_{d}^{+} [kN]	F_{d}^{-} [kN]
B-10-J	Initially identified	16.4	12.19	6.13	2.4	2.2	2.5	1.45	11.4	8.21	5.6	2.93	2.7	5.5	1.81	1.5	11.3	20.6	0.60	80.5	71.3
	Finally updated	7.6	10.19	3.5	2.6	2.5	3.5	2.45	9.2	111.32	7.5	3.9	2.4	3.68	2.42	1.4	5.6	18.3	2.5	71	83
B-12-J	Initially identified	10.5	12.52	5.1	2.33	2.13	3.6	1.35	11.5	18.51	5.48	3.14	2.9	2.5	1.61	2.1	10.3	35.1	1.06	71.2	94.3
	Finally updated	10.3	14.32	4.31	3.25	3.01	4.5	2.43	10.2	16.43	4.4	3.2	3.12	3.4	2.81	1.83	9.56	20.63	0.95	75.64	110.3
B-14-J	Initially identified	10.6	16.05	5.68	2.6	2.4	4.4	1.84	16.6	16.42	6.78	3.42	3.3	3.9	1.82	2.2	10.5	25.5	0.79	81.2	105.2
	Finally updated	13.41	7.56	7.25	0.48	0.32	3.68	2.44	8.56	8.64	6.54	2.83	2.12	3.93	2.54	1.89	15.3	28.23	0.86	112.3	122.2
B-16-J	Initially identified	25.5	17.52	10.13	3.33	3.13	3.1	1.65	12.5	15.51	4.06	3.147	2.85	6.8	1.63	2.5	12	20.3	0.79	77.6	65.3
	Finally updated	14.32	15.63	2.53	1.83	1.32	3.76	2.928	14.32	30.26	1.86	3.82	3.65	3.12	2.13	1.86	13.5	28	2.8	96.3	78.4

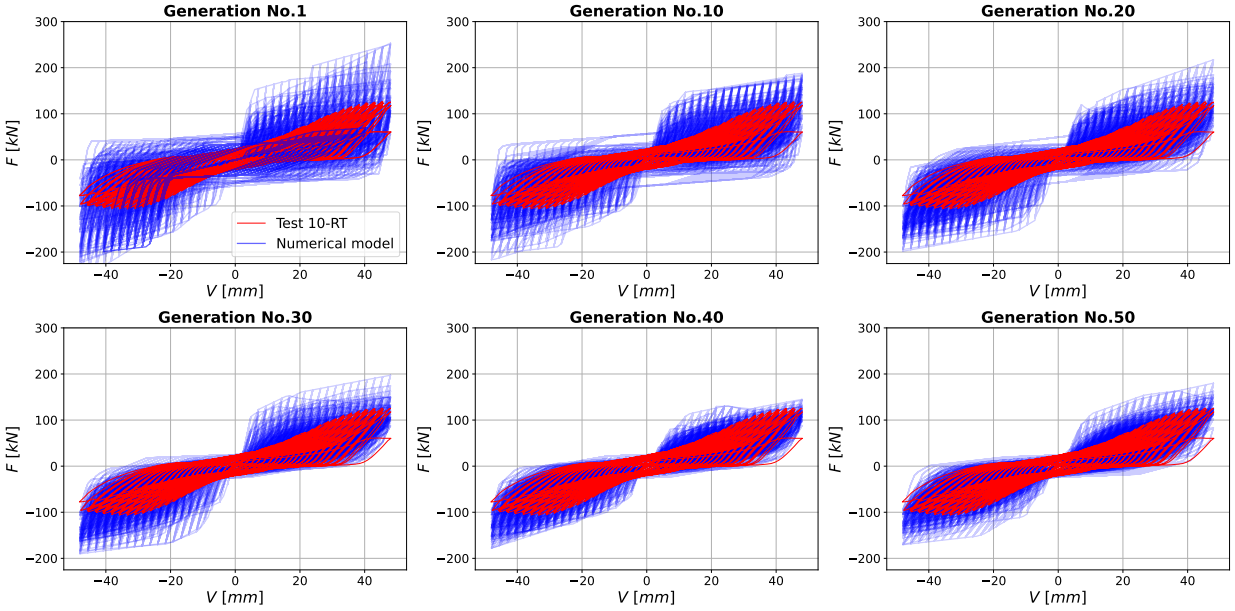

Figure 16: Model updating results over each individual in some generations for Case 10-RT.

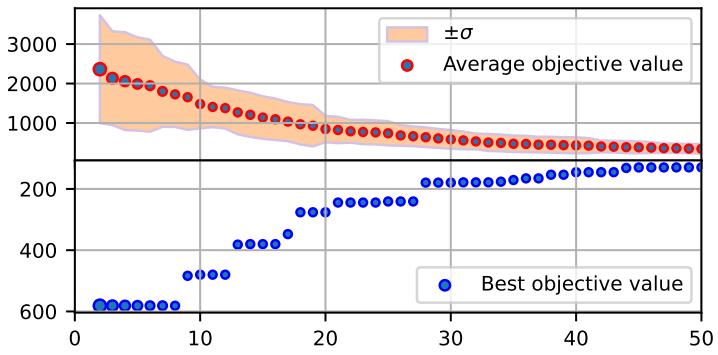

Figure 17: Convergence history of the updating over the objective function evaluation for Case 10-RT.

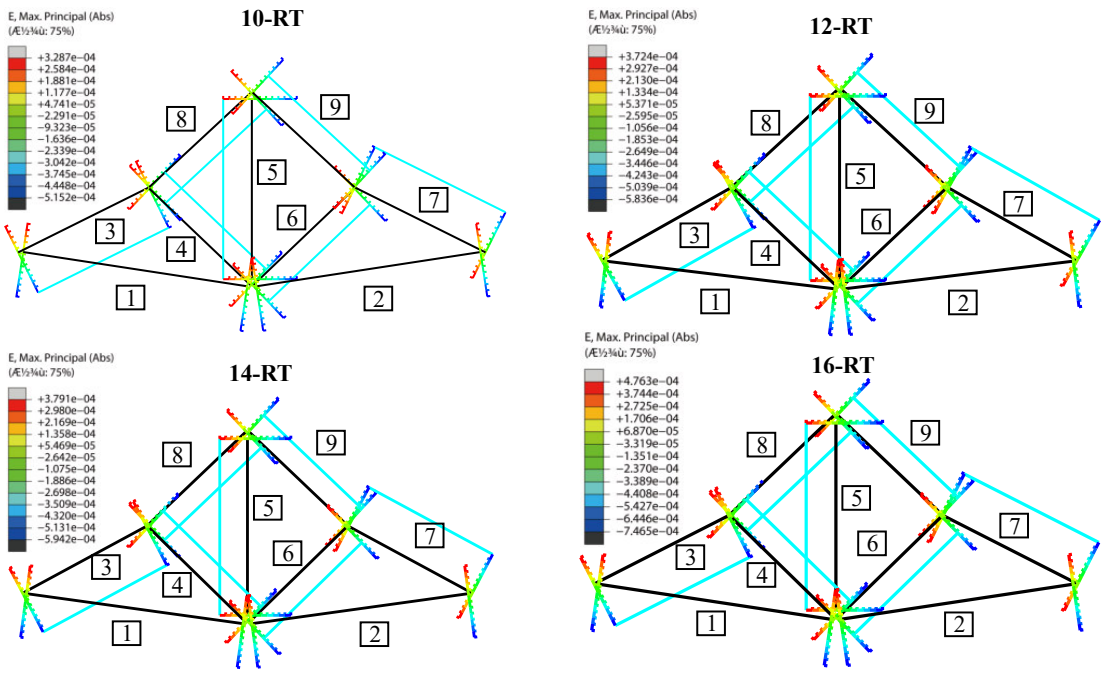

Figure 18: Strain field of each chord at the 25th loading cycle from updated fittest individual.

The initially identified parameters and finally updated parameters values are reported in Table 5. As indicated, the most sensitive parameters are G_1 and G_2 from STOP behavior in S element, which serves to characterize the initial slip behavior caused by the manufacture tolerance between bolt and hole wall. Since planar truss are composed of multiple chords and manufacture tolerance are difficult to keep uniform, these two parameters have the largest relative error between initially identified values and finally updated values. The updating process for Case 10-RT has shown the convergence history illustrated in Figure 17, where the objective function evaluations are reported, and the model updating results over each individual in some representative generations are shown in Figure 16. It can be observed that the updating tends to a stable solution after about 40 generations, 1600 evaluations of individuals. A good agreement between predicted responses from the updated models and test responses were achieved in the last generation. The strain field results of each chord at some loading cycles obtained from the updated fittest roof truss model individual is illustrated in Figure 18. However, compared to the identification results at the joint level, the variance of the identification results at the truss level is larger. This is because the increase in the quantity of observation data points during the optimization process leads to an increase in identification errors. Subsequent improvements can be made by optimizing the population size and optimization generations.

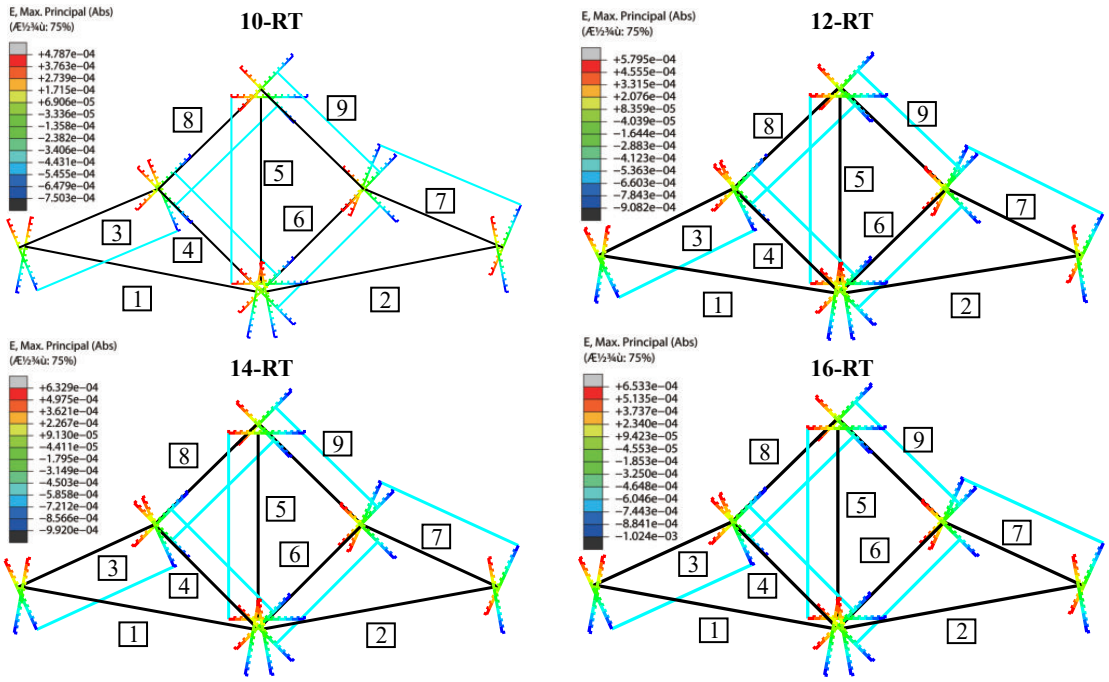

Figure 19: Strain field of each chord at the 60th loading cycle from updated fittest individual.

5.4. Verification of the updated global roof truss model

In last section, four roof truss models were updated according to proposed PGA. In this section, the updated models are further validated against the force-time history, mid-span deflection time series for node 2 and measured strain time series for each chord. More specifically, the finally updated joint model parameters via PGA were used as input for the proposed roof truss model, and the corresponding output responses including force-time history, mid-span deflection time series for node 2 and strain-time series for each chord were obtained and validated against test results.

5.4.1. Comparison of force-time history

The force-time history generated from the updated roof truss models and the corresponding test results are presented in Figure 20. The model has been demonstrated to accurately fit the force-time history. The initial slip and damage behavior can be effectively captured as shown by the force trend in the initial loading cycles, and last cycles respectively. Generally speaking, the developed roof truss models can successfully simulate the pinching and failure behavior of the glubam roof truss.

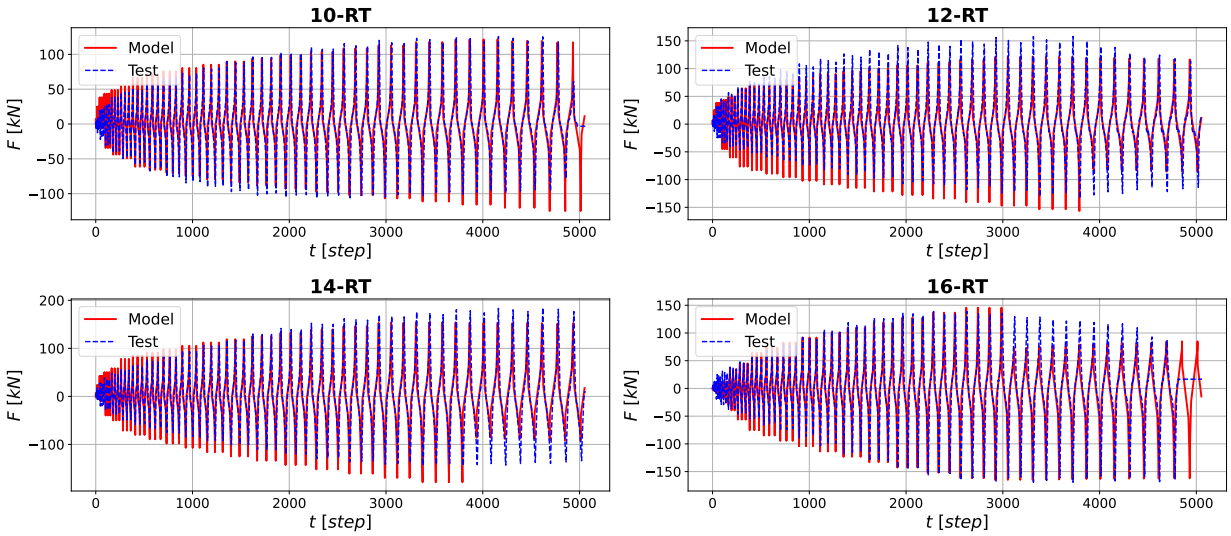

Figure 20: Comparison of force-time history obtained from the model and test.

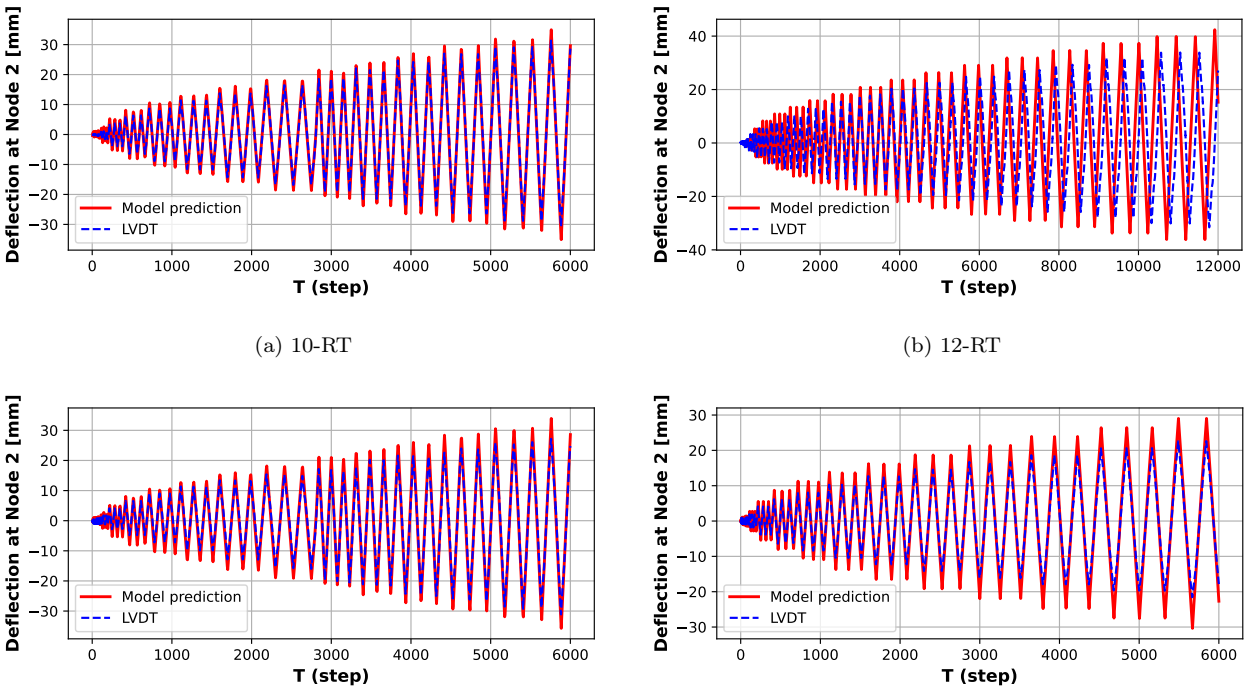

(a) 10-RT

(b) 12-RT

(c) 14-RT

(d) 16-RT

Figure 21: Comparison of mid-span deflection over time at node 2 obtained from the model and test.

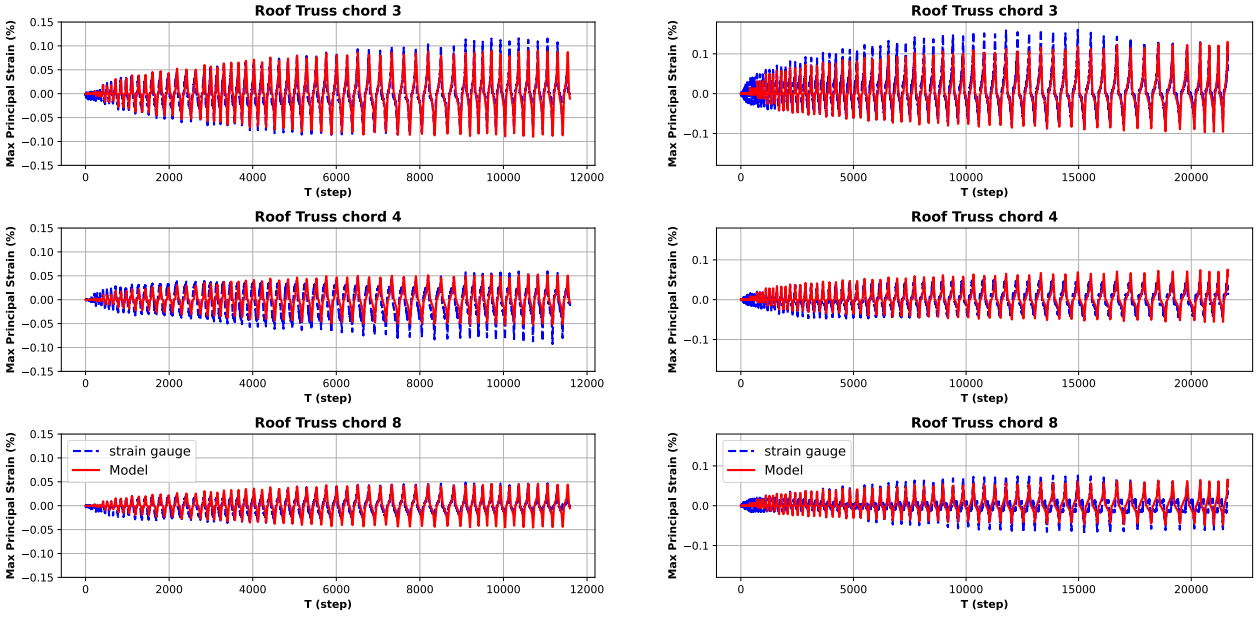

(a) 10-RT

(b) 12-RT

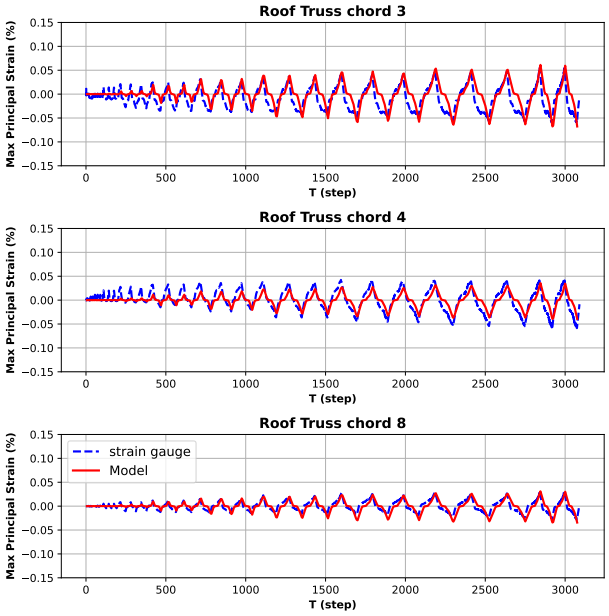

(c) 14-RT

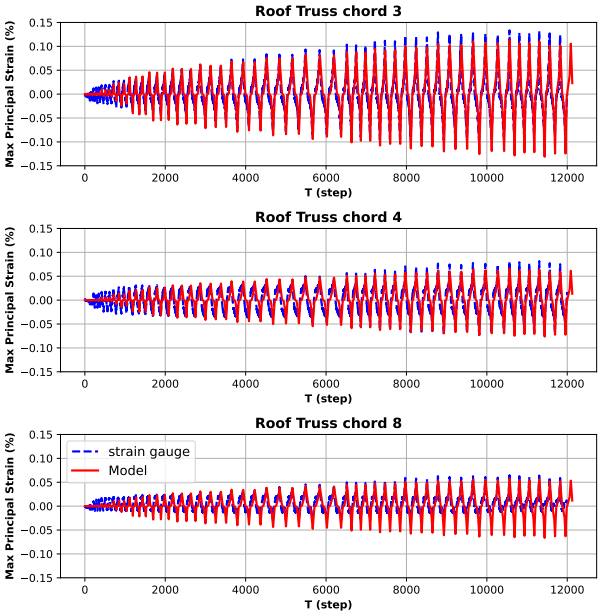

(d) 16-RT

Figure 22: Comparison of strain curves obtained from the model and test for chord 3,4 and 8 of glubam roof truss.

5.4.2. Comparison of mid-span deflection over time at node 2

The result of mid-span deflection over time at node 2 measured by the LVDT is shown in Figure 21. The obtained results are then compared with the corresponding modeling results. Generally, the numerical

results provide a good agreement with test results. It is worth noting that mid-span deflection is an crucial index to evaluate reliability under serviceability limit state (SLS), as defined by [32]. Therefore, it is proved that the proposed models are also feasible for reliability analysis, which will be considered in following research.

5.4.3. Comparison of strain curves for each chord

As an illustrative example, Figure 22 showcases the strain curves over time for each chord of glubam roof truss, as accurately measured by the strain gauge. The obtained strain curves are then compared with the corresponding modeling results, providing a comprehensive assessment of their agreement. Generally, the absolute strain value errors can be controlled within 2×10^{-4}. Additionally, by comparing the strain results for each chord, it can be seen that the internal force of truss chord 3 is the largest, and the failure usually originated from this chord, which is consistent with the experimental observation. Therefore, the accuracy of the proposed model is verified.

6. Conclusions

This study aimed to explore the hysteretic behavior of glubam roof truss structures through a comprehensive experimental and numerical investigation. Specifically, experiments were conducted on four different joint configurations and four types of planar roof truss structures to capture the diverse behaviors exhibited by glubam components. To simulate the complex hysteretic behavior of glubam truss joints accurately, novel mechanics-based models were proposed. These models integrated multi-axial connector and spring elements in series or parallel configurations within the ABAQUS software environment. Additionally, a hybrid numerical model for planar roof truss structures was developed by seamlessly integrating these joint models with truss elements. To facilitate parameter calibration and model updating, a parallel genetic algorithm (PGA) optimization routine was developed and integrated with the ABAQUS software. This innovative approach enabled efficient optimization processes, ensuring the accuracy and reliability of the numerical models. Moreover, this study introduced a novel workflow that merged the capabilities of numerical modeling and optimization using the interactive features of the ABAQUS and Python platforms. Through the incorporation of user-defined programming code, this workflow facilitated seamless integration and enhanced the efficiency of the modeling and optimization processes. Following initial parameter calibration, the predicted responses from the joint models demonstrated good agreement with individual joint test results. Furthermore, through model updating, a more robust global roof truss model was obtained.

The following conclusions were drawn from the study:

- Glubam bolted joints exhibited an asymmetric hysteretic behavior characterized by initial sliding, pinching and damage behavior. Glubam bolted joints majorly performed 3 types of failure pattern

including fracture of bolt, shearing fracture of bolt head and shearing failure of glubam part between two bolts.

- The proposed novel mechanics-based model is capable of simulating sliding, elasticity, plasticity, pinching behavior like most of the existing hysteretic model for wood-based bolt joints. In addition, it can also simulate the asymmetric hysteretic and damage behavior by introducing extra parameters making it superior to other traditional hysteretic models.

- Following preliminary parameter calibration, the proposed model demonstrated relatively accurate simulation of individual joint behavior. Notably, the gaps between bolts and holes created during specimen manufacture, had a significant influence on the performance of the model.

- Model updating resulted in a significant reduction in misfit between the tested and numerically-predicted responses presented by the hybrid roof truss structure. The updated models were validated against tested force-time history, strain field of truss chord and mid-span deflection.

- The multi-threads parallel calibration method based on PGA proposed herein has been proven to be ideal for updating computationally expensive models.

In summary, this study presented a comprehensive approach to investigate and model the hysteretic behavior of glubam roof truss structures. The integration of experimental testing, advanced numerical modeling, and optimization techniques has provided valuable insights into the behavior of these structures, advancing our understanding and facilitating more accurate predictions in engineering practice.

Acknowledgments

This research is supported by the National Key Research and Development Program of China (2019YFD1101002). This work has been partially supported by the Zhejiang University/University of Illinois at Urbana-Champaign Institute.

Declaration of Competing Interest

The authors declare that they have no known competing financial interests or personal relationships that could have appeared to influence the work reported in this paper.

Data availability

The data that support the findings of this study are available from the corresponding author, C.D., upon reasonable request.

References

[1] K. Chung, W. Yu, Mechanical properties of structural bamboo for bamboo scaffoldings, Engineering Structures 24 (2002) 429–442.

[2] L. Villegas, R. Morán, J. J. García, A new joint to assemble light structures of bamboo slats, Construction and Building Materials 98 (2015) 61–68.

[3] Y. Xiao, R. Yang, B. Shan, Production, environmental impact and mechanical properties of glubam, Construction and Building Materials 44 (2013) 765–773.

[4] G. Quaranta, C. Demartino, Y. Xiao, Experimental dynamic characterization of a new composite glubam-steel truss structure, Journal of Building Engineering 25 (2019) 100773.

[5] M. Chen, L. Ye, H. Li, G. Wang, Q. Chen, C. Fang, C. Dai, B. Fei, Flexural strength and ductility of moso bamboo, Construction and Building Materials 246 (2020) 118418.

[6] H. Dong, M. He, X. Wang, C. Christopoulos, Z. Li, Z. Shu, Development of a uniaxial hysteretic model for dowel-type timber joints in opensees, Construction and Building Materials 288 (2021) 123112.

[7] L. Stehn, K. Börjes, The influence of nail ductility on the load capacity of a glulam truss structure, Engineering Structures 26 (2004) 809–816. doi:10.1016/j.engstruct.2004.01.012.

[8] Z. Shu, Z. Li, X. Yu, J. Zhang, M. He, Rotational performance of glulam bolted joints: Experimental investigation and analytical approach, Construction and Building Materials 213 (2019) 675–695.

[9] M. He, J. Luo, D. Tao, Z. Li, Y. Sun, G. He, Rotational behavior of bolted glulam beam-to-column connections with knee brace, Engineering Structures 207 (2020) 110251.

[10] Y. Leng, Q. Xu, K. A. Harries, L. Chen, K. Liu, X. Chen, Experimental study on mechanical properties of laminated bamboo beam-to-column connections, Engineering Structures 210 (2020) 110305.

[11] Z. Shu, B. Ning, J. Chen, Z. Li, M. He, J. Luo, H. Dong, Reinforced moment-resisting glulam bolted connection with coupled long steel rod with screwheads for modern timber frame structures, Earthquake Engineering & Structural Dynamics 52 (2022) 845 – 864.

[12] B.-H. Xu, A. Bouchaïr, M. Taazount, E. J. Vega, Numerical and experimental analyses of multiple-dowel steel-to-timber joints in tension perpendicular to grain, Engineering Structures 31 (2009) 2357–2367.

[13] Z. Guan, P. D. Rodd, Hollow steel dowels — a new application in semi-rigid timber connections, Engineering Structures 23 (2001) 110–119.

[14] M. Izzi, A. Polastri, M. Fragiacomo, Investigating the hysteretic behavior of cross-laminated timber wall systems due to connections, Journal of Structural Engineering-asce 144 (2018) 04018035.

[15] L. F. Sirumbal-Zapata, C. Málaga-Chuquitaype, A. Y. Elghazouli, A three-dimensional plasticity-damage constitutive model for timber under cyclic loads, Computers and Structures 195 (2018) 47–63.

[16] C. Bedon, M. Fragiacomo, Numerical analysis of timber-to-timber joints and composite beams with inclined self-tapping screws, Composite Structures (2019).

[17] C. Mares, J. Mottershead, M. Friswell, Stochastic model updating: Part 1—theory and simulated example, Mechanical Systems and Signal Processing 20 (2006) 1674–1695.

[18] H. H. Khodaparast, J. Mottershead, M. I. Friswell, Perturbation methods for the estimation of parameter variability in stochastic model updating, Mechanical Systems and Signal Processing 22 (2008) 1751–1773.

[19] T. Marwala, Finite Element Model Updating Using Computational Intelligence Techniques: Applications to Structural Dynamics, 2010.

[20] B. Moaveni, X. He, J. P. Conte, J. I. Restrepo, Damage identification study of a seven-story full-scale building slice tested on the ucsd-nees shake table, Structural Safety 32 (2010) 347–356.

[21] G. Di Gangi, C. Demartino, G. Quaranta, G. Monti, Dissipation in sheathing-to-framing connections of light-frame timber shear walls under seismic loads, Engineering Structures 208 (2020) 110246.

[22] P. Racher, K. Laplanche, D. Dhima, A. Bouchaïr, Thermo-mechanical analysis of the fire performance of dowelled timber connection, Engineering Structures 32 (2010) 1148–1157.

[23] B. Do, M. Ohsaki, Bayesian optimization for inverse identification of cyclic constitutive law of structural steels from cyclic structural tests, in: Structures, volume 38, Elsevier, 2022, pp. 1079–1097.

[24] S. Sessa, N. Vaiana, M. Paradiso, L. Rosati, An inverse identification strategy for the mechanical parameters of a phenomenological hysteretic constitutive model, Mechanical Systems and Signal Processing 139 (2020) 106622.

[25] M. Pelliciari, G. Marano, T. Cuoghi, B. Briseghella, D. Lavorato, A. Tarantino, Parameter identification of degrading and pinched hysteretic systems using a modified bouc–wen model, Structure and Infrastructure Engineering 14 (2018) 1–13.

[26] R. Astroza, H. Ebrahimian, J. P. Conte, Material parameter identification in distributed plasticity fe models of frame-type structures using nonlinear stochastic filtering, Journal of Engineering Mechanics 141 (2015) 04014149.

[27] R. Astroza, A. Alessandri, J. P. Conte, A dual adaptive filtering approach for nonlinear finite element model updating accounting for modeling uncertainty, Mechanical Systems and Signal Processing 115 (2019) 782–800.

[28] H. Ebrahimian, R. Astroza, J. P. Conte, R. A. de Callafon, Nonlinear finite element model updating for damage identification of civil structures using batch bayesian estimation, Mechanical Systems and Signal Processing 84 (2017) 194–222.

[29] T. Vallée, T. Tannert, S. Hehl, Experimental and numerical investigations on full-scale adhesively bonded timber trusses, Materials and Structures 44 (2011) 1745–1758.

[30] S. Šilih, M. Premrov, S. Kravanja, Optimum design of plane timber trusses considering joint flexibility, Engineering Structures 27 (2005) 145–154.

[31] Y. Xiao, G. Chen, L. Feng, Experimental studies on roof trusses made of glubam, Materials and Structures 47 (2013) 1879–1890.

[32] GB50005, Code for design of timber structures, 2017.

[33] E. C. for Standardization (CEN), Timber structures-test methods-cyclic testing of joints made with mechanical fasteners, European Standard. 2001;12512 (2001).

[34] G. C. Marano, G. Quaranta, J. Avakian, A. Palmeri, Identification of passive devices for vibration control by evolutionary algorithms, 2013.

[35] R. Greco, J. Avakian, G. Marano, A comparative study on parameter identification of fluid viscous dampers with different models, Archive of Applied Mechanics 84 (2014). doi:10.1007/s00419-014-0869-3.

[36] V. Skorpil, V. Oujezsky, P. Cika, M. Tuleja, Parallel processing of genetic algorithms in python language, in: 2019 PhotonIcs and Electromagnetics Research Symposium, 2019, pp. 3727–3731.

[37] O. Hasançebi, T. Bahçecioğlu, Ö. Kurç, M. Saka, Optimum design of high-rise steel buildings using an evolution strategy integrated parallel algorithm, Computers and Structures 89 (2011) 2037–2051.

[38] D. Shi, C. Demartino, Z. Li, Y. Xiao, Axial load–deformation behavior and fracture characteristics of bolted steel to laminated timber and glubam connections, Composite Structures 305 (2023) 116486.

[39] D. Shi, H. Huang, N. Li, Y. Liu, C. Demartino, Bolted steel to laminated timber and glubam connections: Axial behavior and finite-element modeling, International Journal of Mechanical Sciences 252 (2023) 108364.

[40] G. Quaranta, G. C. Marano, R. Greco, G. Monti, Parametric identification of seismic isolators using differential evolution and particle swarm optimization, Applied Soft Computing 22 (2014) 458–464.

Appendix A. Flowchart of the proposed parallel algorithm

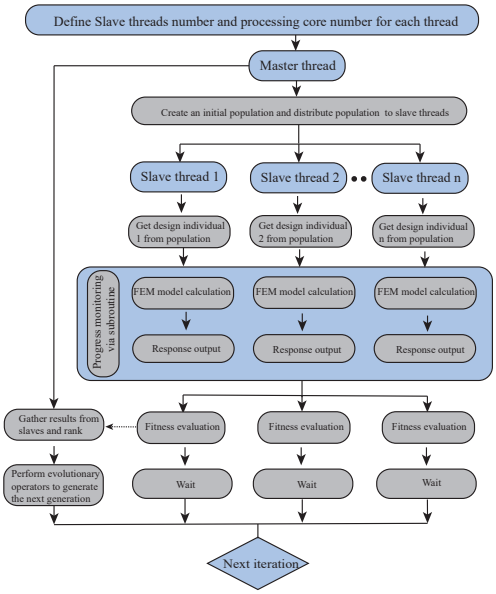

Figure A.23: Flowchart of the proposed parallel algorithm.

Appendix B. Identification framework

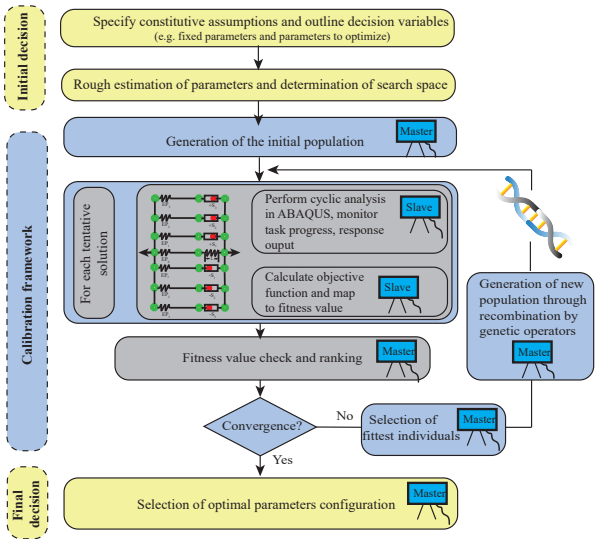

Figure B.24: Flowchart of the calibration framework (adapted from Quaranta et al. [40], Pelliciari et al. [25]).